University of Zurich

Department of Physics

Application of a Closed-Form Population-Based Tumor Control Probability Model

Master's Thesis

Sara Erni

Supervisors	Prof. Dr. Uwe Schneider
	Katerine Viviana Diaz Hernandez
Field of Study	Medical Physics
Contact Details	sara.erni@uzh.ch
Matriculation Number	19-742-964
Submission Date	05.12.2024

Abstract

Tumor control probability (TCP) models are essential for evaluating radiotherapy treatment results and optimizing fractionation schedules. In this thesis, a closed-form population-based TCP model is applied to clinical data from four different tumor sites: pyriform sinus, breast, non-small cell lung cancer (NSCLC) and brain metastases. The TCP model was fitted to the data using two survival models, the linear-quadratic (LQ) and the track-event (TE) model. Furthermore, the risk of symptomatic radiation necrosis is modeled for brain metastases, where high-dose treatments are common. By combining the TCP model with models predicting symptomatic radiation necrosis, we employ the concept of complication-free tumor control probability. This metric is used to quantify the probability of tumor control without significant side effects. It provides a promising method to optimize fractionation schedules for brain metastases. For breast cancer, the TCP model is used to calculate the microscopic residual tumor volume after surgery for individual patients, enabling the prediction of TCP outcomes following adjuvant radiotherapy. When comparing the results of the LQ and the TE model, both models exhibit comparable performance in fitting the data. However, further validation on larger, more diverse datasets is necessary to confirm the accuracy of the TE model.

Acknowledgements

A big thank you goes to my supervisors Uwe and Katerine. Working with them was always very pleasant. They always took the time to answer my questions, even the silly ones. I always appreciated the lunches we had together in the office. Thanks to you, I had the opportunity to do my Master's thesis in such an exciting field, which taught me a lot. I would also like to thank Jan for answering my questions about the maximum likelihood estimation method. Thanks also to Christof, who took away some of my fear of the Master's examination and supported me in the area of error calculation. Finally, I would like to thank my family and friends who have always supported me and believed in me.

Contents

1 Introduction . . . 1
2 Materials and Methods . . . 3
2.1 Models of Cell Survival . . . 3
2.1.1 Linear-Quadratic Model . . . 3
2.1.2 Track-Event Model . . . 6
2.2 Models of Tumor Control Probability . . . 10
2.2.1 Local Control and TCP . . . 11
2.3 Data Search and Collection . . . 12
2.3.1 Dose Estimation . . . 12
2.3.2 Volume Estimation . . . 13
2.3.3 Collection of Local Control Data . . . 14
2.4 Tumor Sites . . . 14
2.4.1 Pyriform Sinus . . . 15
2.4.2 Breast . . . 16
2.4.3 NSCLC . . . 19
2.4.4 Brain Metastases . . . 23
2.5 Optimizing Model Parameters with Maximum Likelihood Method . . . 26
2.6 Visualization . . . 28
2.7 Radiation Necrosis . . . 29
2.7.1 Models of Symptomatic Radiation Necrosis Probability . . . 30
2.8 Complication-free Tumor Control . . . 33
3 Results . . . 34
3.1 Pyriform Sinus . . . 35
3.2 Breast . . . 38
3.2.1 Volume Data . . . 38
3.2.2 Dose Data . . . 40
3.3 NSCLC . . . 42
3.4 Brain Metastases . . . 45
3.5 Model Performance Analysis . . . 48
3.6 Radiation Necrosis . . . 48
3.6.1 Single-Fraction Treatments . . . 48
3.6.2 Multi-Fraction Treatments . . . 50
3.7 Complication-free Tumor Control . . . 52
4 Discussion . . . 54
4.1 Tumor-Specific Findings . . . 54
4.1.1 Pyriform Sinus . . . 54

4.1.2 Breast 55
4.1.3 NSCLC 56
4.1.4 Brain Metastases and Symptomatic Radiation Necrosis 57
4.2 Model Comparison and Outlook 59
4.3 Biological Considerations and Model Limitations 60
A Appendix 61
A.1 Initial Parameter Ranges for Maximum Likelihood Optimization 61
A.2 Summary of Estimated Model Parameters 62
A.3 TCP in Brain Metastases as a Function of Tumor volume 63
A.4 Gaussian Error Propagation 64
Bibliography 66

1 Introduction

One of the main goals of radiotherapy is to effectively control tumors. The *tumor control probability (TCP)* serves as a primary endpoint for treatment evaluation. Models describing TCP allow clinicians to predict the likelihood of successful tumor control and quantify the effects of different fractionation schedules.

Building on this foundation, a novel TCP population model that integrates tumor volume variations and cell sensitivity differences within a patient population [1] is presented in this thesis. This mechanistically-based model allows for simultaneous analysis of dose and tumor volume effects on treatment outcomes. Interpatient variations, such as differences in tumor size and sensitivity, significantly affect dose-response outcomes. Without considering these factors, the fitted radiobiological parameters and the respective TCP curves are biased. Building on the work of Radonic et al. [2], who developed a model that incorporates tumor volume heterogeneity, the approach presented in this thesis extends these ideas to include variations in both tumor volume and cell sensitivity. In addition, we present an empirical consideration of the evolution in time of *local control (LC)* in terms of TCP [1], which allows to track how well a tumor is controlled over time.

TCP models are generally based on survival models, with the *linear-quadratic (LQ)* model being one of the most widely used in radiotherapy. It is employed to calculate isoeffect doses, i.e. doses that produce the same biological effect on tissue, for various fractionation schemes. The radiotherapeutic response, both for tumor control and for complications, is dominated by cell killing, with the LQ model serving as a mechanistic framework for describing this process. The research by Brenner et al. [3] supports the effectiveness of the LQ model, showing that it reliably predicts dose-response relationships both *in vitro* and *in vivo*, particularly within a dose-per-fraction range of 2-15 Gy (Gray). They observed that the model's predictions align well with actual patient outcomes, with no evidence of underdosing or overdosing across various fractionation regimes.

However, other studies question the effectiveness of the LQ model at high doses. Classical cell-survival curves exhibit an increasingly exponential trend at higher doses per fraction, like those seen in *stereotactic body radiotherapy (SBRT)*. Research by Sheu et al. [4] suggests that the LQ model would underestimate the dose needed to achieve tumor control in treatments with large fractions. Their results support the hypothesis that at higher doses, where cell survival transitions to an exponential behavior pattern, the LQ model becomes less reliable.

To address these limitations, Besserer et al. [5] propose an alternative survival model, known as the *track-event (TE)* model. Unlike the LQ model, the TE model shows exponential survival at high doses, which may provide a closer match to how cells respond. Since the TE model provides a more mechanistically grounded description of dose-response, it potentially offers a more accurate approach for high-dose treatments compared to the empirically-based LQ model. At low doses, the LQ model is a good approximation of the TE model. While some argue that the LQ model's extensive clinical application and lack of observed treatment failures justify its continued use, others highlight deviations at higher doses as evidence that the LQ model may not be universally applicable. The contrasting evidence suggests that the examination of alternative models could improve the accuracy of the TCP predictions.

To validate the developed population LC model, which incorporates TCP, clinical data from four tumor sites are analyzed in this thesis: *pyriform sinus*, *breast*, *non-small cell lung cancer (NSCLC)* and *brain metastases*. The LQ model and the TE model, which are introduced in Chapter 2, are used to fit the collected datasets. For NSCLC, both conventional fractionated and hypofractionated treatments are analyzed, which allows for a detailed comparison of the two models. In the case of brain metastases, treatments like *stereotactic radiosurgery (SRS)* and *fractionated stereotactic radiation therapy (fSRT)* are common. Although these high-dose therapies are effective, they also carry risks, with *radiation necrosis (RN)* being a well-known side effect. To calculate the probability of such complications, two simple models of *symptomatic radiation necrosis probability (P_{SRN})* are used: a logistic model and its logarithmic form. These models, also introduced in Chapter 2, let us predict the risk of symptomatic radiation necrosis based on clinical data. The results of these analyses are presented in Chapter 3 and discussed in Chapter 4.

By combining the TCP and P_{SRN} models, along with the parameters obtained from their fits, we define the *complication-free tumor control probability*. This represents the probability of achieving tumor control without significant radiation-induced complications, such as symptomatic necrosis. The analysis of this combined metric, discussed in detail in Chapter 4, is crucial for identifying the best fractionation schedules for brain metastases based on tumor size and the risk of side effects.

2 Materials and Methods

This chapter provides a comprehensive overview of the methodologies and approaches used to model tumor control and related complications in radiation therapy. We start by introducing two widely used survival models based on Poisson statistics that are fundamental in predicting cell survival after radiation exposure. These models serve as the basis for the development of the novel tumor control probability population model, which is presented for both survival models in Section 2.2. In addition, we present the empirical assessment of local control over time in terms of TCP, providing insights into how tumor control evolves after treatment. This is followed by a detailed description of the data collection process in Section 2.3. The subsequent Section 2.4 focuses on the different tumor sites and presenting the collected data. Following this, we explain the use of the maximum likelihood estimation method for optimizing the model parameters, ensuring the most accurate fitting of the data to the respective models. We shift to the visualization of the data in Section 2.6, detailing how plots are generated and presented in the results chapter. Section 2.7 is dedicated to the issue of symptomatic radiation necrosis, a common complication following stereotactic radiosurgery. Two simple models for symptomatic radiation necrosis are described. Finally, the chapter concludes with the combination of the TCP model and symptomatic radiation necrosis models, employing the concept of complication-free TCP, which quantifies the likelihood of achieving tumor control without complications.

2.1 Models of Cell Survival

The *linear-quadratic (LQ)* model and the *track-event (TE)* model play a crucial role in radiobiology. They quantify the relationship between radiation dose and biological response in terms of cell survival. The LQ model is distinguished by its simplicity and adaptability over a wide range of dose levels, while the TE model provides a more detailed mechanistic approach, taking into account specific interactions at the cellular level.

2.1.1 Linear-Quadratic Model

The LQ model describes the fraction of surviving cells S as a function of the total radiation dose D, parametrized by the radiosensitivity parameters α and β:

$$S(D, \alpha, \beta) = e^{-\alpha D - \beta D^2}. \tag{2.1}$$

In this equation, the parameter α represents the linear contribution to cell death, caused primarily by direct DNA damage, while the parameter β accounts for the quadratic contribution, reflecting indirect damage from DNA repair mechanisms and cell repopulation [6]. The survival curve in Figure 1 illustrates this relationship described by the LQ model. At low doses, the linear term αD dominates, producing a shoulder on the curve that reflects a phase where cells can repair sublethal DNA damage. As the dose increases, the quadratic term βD^2 becomes more significant, resulting in a steeper, quadratic decline in survival. The dose at which the linear and quadratic contributions to cell damage are equal corresponds to the $\frac{\alpha}{\beta}$ ratio. This key quantity derived from the LQ model has units of Gray (Gy) and is important for understanding tissue response to radiation.

The significance of the $\frac{\alpha}{\beta}$ ratio becomes even more apparent when considering the variability between different tissues, reflecting their different sensitivities to radiation. Normal tissues, which typically have low $\frac{\alpha}{\beta}$ values, are more sensitive to the effects of fractionation, meaning that the application of lower doses over multiple fractions is beneficial. Conversely, tumors or rapidly proliferating normal tissues tend to have higher $\frac{\alpha}{\beta}$ ratios, indicating less dependence on fraction size for therapeutic effect. Understanding the $\frac{\alpha}{\beta}$ ratio of different tissues helps clinicians optimize treatment plans to maximize tumor control while minimizing damage to surrounding normal tissues. For a single-fraction treatment, the total dose D in Equation (2.1) is equal to the dose per fraction, denoted as d_s, and we get

$$S(d_s, \alpha, \beta) = e^{-\alpha d_s - \beta d_s^2}. \tag{2.2}$$

To account for fractionated treatments, where the total dose is delivered in n fractions, we extend the survival function to

$$S(n, d_f, \alpha, \beta) = e^{-n\left(\alpha d_f + \beta d_f^2\right)}, \tag{2.3}$$

where d_f is the dose per fraction. The total dose delivered over the entire treatment time is then given by $D = n\, d_f$. Substituting this into Equation (2.3) we obtain the survival function in terms of the total dose and the dose per fraction:

$$S(D, d_f, \alpha, \beta) = e^{-D\left(\alpha + \beta d_f\right)}. \tag{2.4}$$

The LQ model is primarily used to estimate equivalent radiotherapy schedules that achieve the same biological effect. To find the *equivalent total dose (EQDX)* delivered

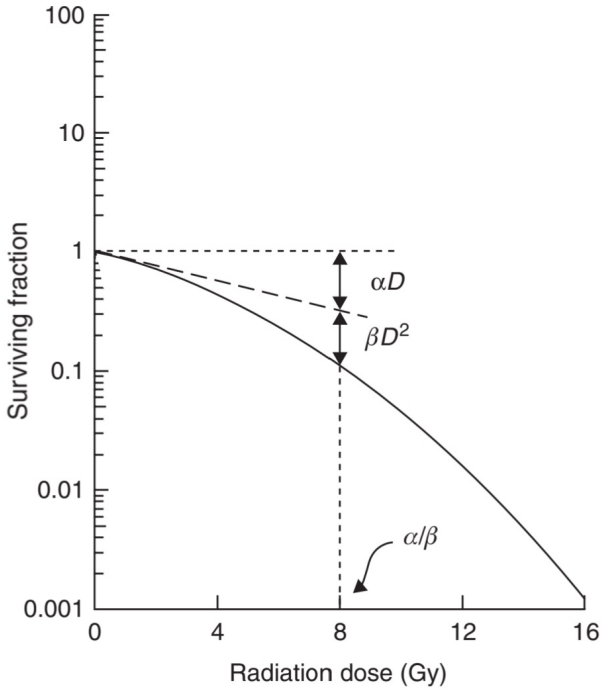

Figure 1 Cell survival curve illustrating the relationship between radiation dose and the fraction of surviving cells. The curve is based on the linear-quadratic (LQ) model, where the total radiation dose D induces both linear (αD) and quadratic (βD^2) contributions to cell damage. At lower doses, the linear term dominates, while the quadratic term becomes more significant at higher doses, resulting in a steeper decline in cell survival. The $\frac{\alpha}{\beta}$ ratio, marked on the curve, represents the dose at which the linear and quadratic effects are equal, serving as a key quantity for understanding tissue response to radiation. Figure adapted from [7].

at a dose per fraction X, we equate the survival functions for two different treatment regimens:

$$e^{-D\left(\alpha+\beta d_f\right)} = e^{-\mathrm{EQDX}\,(\alpha+\beta \mathrm{X})}, \tag{2.5}$$

where D is the total dose corresponding to the dose per fraction d_f of the original treatment regimen. Solving for EQDX yields:

$$\mathrm{EQDX} = D\,\frac{\left(1+\frac{d_f}{\alpha/\beta}\right)}{\left(1+\frac{\mathrm{X}}{\alpha/\beta}\right)}. \tag{2.6}$$

In clinical practice, X is typically set at 2 Gy, known as standard fractionation. Equation (2.6) enables the conversion of doses between different fractionation schedules while maintaining a constant biological effect.

For certain cancer types, *stereotactic body radiotherapy (SBRT)* is a commonly used treatment method. SBRT delivers a high dose of radiation in a single or a few fractions, typically within 1 to 5 sessions, as opposed to the multiple fractions used in conventional

radiotherapy. However, due to the high dose per fraction, there is an increased risk of toxicity, which will be discussed more detailed in Section 2.7. To convert the dose from a multi-fraction treatment to an equivalent single-fraction treatment, we equate the survival function for a single-fraction treatment (Equation (2.2)) to the survival function for a multi-fraction treatment with n fractions of dose d_f (Equation (2.3)):

$$e^{-\alpha d_s - \beta d_s^2} = e^{-n\left(\alpha d_f + \beta d_f^2\right)}. \tag{2.7}$$

We aim to solve this equation for the single-fraction dose d_s. By applying the quadratic formula, we obtain the following solution:

$$d_s = \frac{-\frac{\alpha}{\beta} + \sqrt{\left(\frac{\alpha}{\beta}\right)^2 + 4n\, d_f\, \frac{\alpha}{\beta} + 4n\, d_f^2}}{2}. \tag{2.8}$$

This formula allows us to calculate the single-fraction dose d_s that yields the same biological effect as a multi-fraction treatment with n fractions of d_f.

2.1.2 Track-Event Model

The primary target of energy deposition within cells during radiation treatment is chromosomal DNA. Significant damage is manifested as *double-strand breaks (DSBs)*, i.e. a type of severe DNA damage in which both strands of the DNA helix are broken. The assumptions to model this energy deposition are [5]:

- **Definition of a track:** The passage of high-energy particles (charged or uncharged) and their resulting secondary particles form a track.
- **DSB production:** Tracks can cause one or more DSBs either directly by ionization or indirectly by generating free radicals in the environment of the DNA.
- **Definition of an event:** The occurrence of two DSBs on the same or different chromosomes defines an event and is always lethal. One single DSB is not lethal and is therefore not considered an event.

As shown in Figure 2, events can be generated by two different mechanisms: *one-track events (OTEs)* and *two-track events (TTEs)*:

- **One-Track Event (OTE):** In this mechanism, one track produces two DSBs, resulting in a lethal event.
- **Two-Track Event (TTE):** Each track causes a single DSB. A lethal event requires at least two TTEs on the same or different chromosomes.

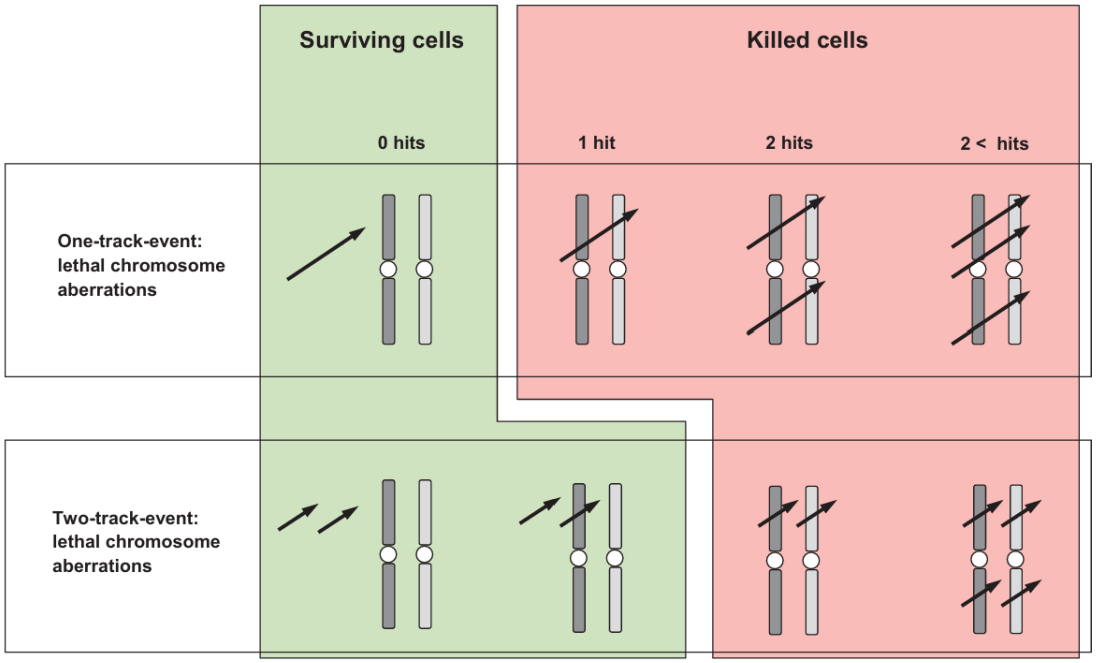

Figure 2 Schematic representation of DNA double-strand breaks and their contribution to cell survival or death through one-track events (OTEs) and two-track events (TTEs). The green region on the left represents surviving cells, where no hits or only one hit from a two-track event results in cell survival. In the case of OTEs, a single hit causes two DSBs, leading to lethal chromosomal aberrations (shown in red). TTEs require at least two independent hits to kill the respective cell. Figure adapted from [5].

The stochastic nature of cell killing following these events can be modeled using the Poisson distribution, assuming a large number of irradiated cells and a low probability of hitting the target. The distribution of cells with no hits $N(0)$ and one hit $N(1)$ is given by

$$N(0) = N_0\, e^{-x}, \tag{2.9}$$

$$N(1) = N_0\, x\, e^{-x}, \tag{2.10}$$

where N_0 is the initial number of cells and x is the mean number of hits. For OTEs, one hit corresponds to a lethal event (two DSBs), while for TTEs one hit corresponds to a single DSB. The mean number of hits x is proportional to the dose D:

$$x = p\, D \text{ for OTEs}, \tag{2.11}$$

$$x = q\, D \text{ for TTEs}, \tag{2.12}$$

where p and q represent the probabilities of lethal events and DSBs, respectively. A cell survives if it experiences no OTE or at most one TTE. The survival probability

S is therefore the product of the probability of no OTE, denoted $P_{\mathrm{OTE}}(0)$, and the probability of at most one TTE, denoted $P_{\mathrm{TTE}}(0 \cup 1)$:

$$S = P_{\mathrm{OTE}}(0) \times P_{\mathrm{TTE}}(0 \cup 1) \tag{2.13}$$

with

$$P_{\mathrm{TTE}}(0 \cup 1) = P_{\mathrm{TTE}}(0) + P_{\mathrm{TTE}}(1), \tag{2.14}$$

where $P_{\mathrm{TTE}}(0)$ is the probability of no TTE and $P_{\mathrm{TTE}}(1)$ is the probability of one TTE. Combining Equation (2.9) and (2.11), and assuming that the survival probability is proportional to the ratio of surviving cells to the total cell population, the probability of no OTE is given by:

$$P_{\mathrm{OTE}}(0) = e^{-pD}. \tag{2.15}$$

Using Equation (2.9), (2.10) and (2.14) we get the probability that a cell will receive at most one TTE:

$$P_{\mathrm{TTE}}(0 \cup 1) = e^{-qD} + qDe^{-qD} = (1 + qD)e^{-qD}. \tag{2.16}$$

The total probability of cell survival according to Equation (2.13) is therefore

$$S(D, q, p) = (1 + qD)e^{-(q+p)D}, \tag{2.17}$$

which can be re-written as

$$S(D, q, p) = e^{\log(1+qD)}e^{-(q+p)D}. \tag{2.18}$$

A taylor expansion of the logarithm, based on the area hyperbolic tangent function, results in the low dose approximation

$$S(D, q, p) = e^{-q\left(\frac{D^2}{D+\frac{2}{q}}\right)-pD}. \tag{2.19}$$

The dose at which OTEs and TTEs are equally likely corresponds to the $\frac{\alpha}{\beta}$ ratio in the LQ model, where the linear and quadratic contributions to cell damage are balanced. Since no analytical solution can be obtained by equalizing Equation (2.15) and (2.16), we use the low dose approximation (Equation (2.19)) to find the parameter q in terms of p and the $\frac{\alpha}{\beta}$ ratio of the LQ model. Equalizing the q-dependent and p-dependent terms within Equation (2.19) and solving for q, we obtain:

$$q(p, \alpha/\beta) = \frac{1}{2}\left(p + \frac{1}{\alpha/\beta}\sqrt{(p\ \alpha/\beta)^2 + 8p\ \alpha/\beta}\right). \tag{2.20}$$

For a single-fraction treatment, the total dose D in Equation (2.17) is equal to the dose per fraction d_s:

$$S(D,q,p) = (1+qd_s)e^{-(q+p)d_s}. \tag{2.21}$$

If we have multiple fractions, we rewrite Equation (2.21) in terms of dose per fraction d_f by raising it to the power of n and using the relationship $D = n\,d_f$,

$$S(D,d_f,q,p) = (1+qd_f)^{\frac{D}{d_f}} e^{-(q+p)D}. \tag{2.22}$$

To transform different fractionation schedules, we can calculate the isoeffect formula. Assuming that two different fractionation schedules give the same survival,

$$\left((1+qd_f)e^{-(q+p)d_f}\right)^{\frac{D}{d_f}} = \left((1+qX)e^{-(q+p)X}\right)^{\frac{\mathrm{EQDX}}{X}}, \tag{2.23}$$

we get the equivalent total dose delivered at a dose per fraction X:

$$\mathrm{EQDX} = D\,\frac{\frac{1}{d_f}\log(1+qd_f) - q - p}{\frac{1}{X}\log(1+qX) - q - p}. \tag{2.24}$$

In the next step, we want to determine the single-fraction equivalent dose for stereotactic body radiotherapy treatments modeled by the TE model. Following the same principles as in the LQ model, we begin by equating the survival function for a single-fraction treatment (Equation (2.21)) to that of a multi-fraction treatment with n fractions of dose d_f (Equation (2.22)):

$$(1+qd_s)e^{-d_s(q+p)} = (1+qd_f)^n e^{-nd_f(q+p)}. \tag{2.25}$$

To solve this equation analytically for d_s, we need to use the Lambert W function, denoted as $W(x)$, which is the inverse of the function xe^x. This function is particularly useful in our case, because the unknown variable appears inside an exponential function as well as a multiplicative term. The Lambert W function provides a way to isolate the variable d_s:

$$d_s = -\frac{1}{q}\Bigg(-1+\left(\frac{n+qnd_f}{n}\right)^n \times \exp\left[\frac{-W\left(-\frac{1}{q}\left(\frac{n+qnd_f}{n}\right)^n (p+q)e^{-\frac{(p+q)(qnd_f+1)}{q}}\right)q - (p+q)(qnd_f+1)}{q}\right]\Bigg). \tag{2.26}$$

2.2 Models of Tumor Control Probability

The likelihood that no tumor cell survives after exposure to a given radiation dose is quantified using Poisson statistics. This approach assumes that the survival of a tumor cell is a rare event and that the initial number of tumor cells is large. Under these conditions, the TCP for an individual patient can be expressed as [8]

$$\mathrm{TCP} = e^{-N_S}, \tag{2.27}$$

where N_S represents the number of tumor cells that survive after radiation exposure. The value of N_S is determined as the product of the initial number of tumor cells N_0 and the survival fraction S, which depends on the chosen survival model. Substituting $N_S = N_0 S$ into Equation (2.27) and expressing N_0 as the product of the number of tumor cells per unit volume ρ and the tumor volume V, the TCP becomes [9]

$$\mathrm{TCP} = e^{-\rho V S}. \tag{2.28}$$

In a population, tumors vary in size. As shown in Radonic et al [2], an exponential distribution of tumor volumes [10]

$$f_{\bar{V}}(V) = \frac{1}{\bar{V}} e^{-\frac{V}{\bar{V}}} \tag{2.29}$$

can be inserted into Equation (2.28). The average tumor volume of the population is denoted by $\bar{V}$. Assuming a constant clonogenic density of 10^7 cm^{-3}, the resulting TCP from a population is given by

$$\mathrm{TCP}_{\mathrm{pop}} = \int_0^\infty e^{-\rho V S} \frac{1}{\bar{V}} e^{-\frac{V}{\bar{V}}} \, dV = \frac{1}{1 + \rho \bar{V} S}. \tag{2.30}$$

Integration yields the logistic model previously used by Okunieff et al. [11] without further mechanistic justification.

In order to make the model more accurate, we will additionally assume a variation in cell radiosensitivity α [1]. We consider a uniform distribution between a minimum value $\alpha_{min} = \alpha - \sigma_\alpha$ and a maximum value $\alpha_{max} = \alpha + \sigma_\alpha$, where σ_α is the variation of radiosensitivity from the central value α. Performing the integration over α in the following expression:

$$\mathrm{TCP}_{\mathrm{pop}} = \frac{1}{2\sigma_\alpha} \int_{\alpha_{min}}^{\alpha_{max}} \frac{1}{1 + \rho \bar{V} S} \, d\alpha, \tag{2.31}$$

where we have taken into account the normalization factor $\frac{1}{2\sigma_\alpha}$, we obtain

$$\mathrm{TCP}_{\mathrm{pop}} = \frac{1}{2\sigma_\alpha D} \log\left(\frac{\rho \bar{V} + e^{D(\alpha + \sigma_\alpha + \beta d_f)}}{\rho \bar{V} + e^{D(\alpha - \sigma_\alpha + \beta d_f)}} \right), \tag{2.32}$$

for the LQ model. In the TE model, where the integration is done for $p_{min} = p - \sigma_p$ and $p_{max} = p + \sigma_p$, we end up with:

$$\mathrm{TCP}_{\mathrm{pop}} = \frac{1}{2\sigma_p D} \log\left(\frac{\rho \bar{V}(1+qd)^{\frac{D}{d_f}} + e^{D(p+\sigma_p+q)}}{\rho \bar{V}(1+qd)^{\frac{D}{d_f}} + e^{D(p-\sigma_p+q)}} \right). \tag{2.33}$$

2.2.1 Local Control and TCP

Local control is defined as the the successful treatment of a tumor within a defined treatment area and the prevention of its regrowth or recurrence at the original site. In the context of radiotherapy, local control is achieved when the tumor cells in the target region have been effectively destroyed or their proliferation has been stopped. This is confirmed by clinical assessments and imaging studies over a defined period of follow-up. Local control and tumor control probability are closely related concepts in radiotherapy. While local control is an observed clinical outcome, TCP is a theoretical concept used to predict this outcome after a predefined follow-up time. Effective treatment planning relies on accurate TCP models to maximize the likelihood of achieving local control. In clinical observations, local control tends to stabilize over longer follow-up periods. To replicate this trend, LC is expressed as a decreasing exponential function of follow-up time. It is assumed that for an infinite follow-up time, LC approaches the constant average value $\mathrm{TCP}_{\mathrm{pop}}$. This is written as [1]:

$$\mathrm{LC} = \left(1 - \mathrm{TCP}_{\mathrm{pop}}\right) e^{-\lambda t} + \mathrm{TCP}_{\mathrm{pop}}, \tag{2.34}$$

where λ is the local control rate and t is the follow-up time. Using λ we can determine

$$t_{1/2} = \frac{\log 2}{\lambda} \tag{2.35}$$

which represents the characteristic time at which LC approaches $\mathrm{TCP}_{\mathrm{pop}}$ (see Figure 3).

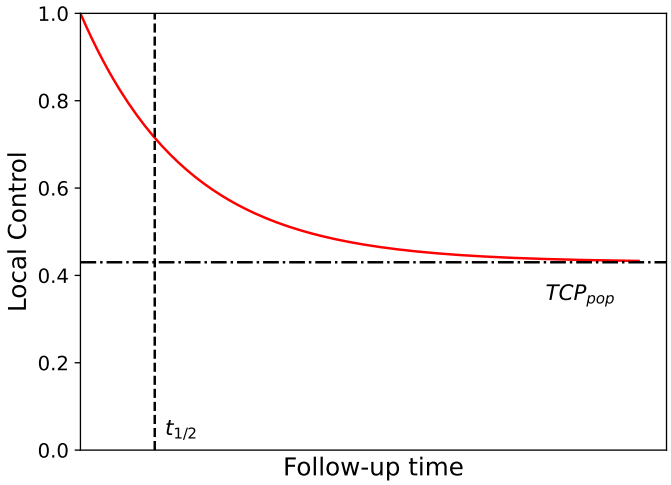

Figure 3 Exponential model of local control as a function of follow-up time. The red curve illustrates the decline in local control over time (Equation (2.34)) for patients who are not cured. After a certain follow-up period, LC emerges as the constant $\mathrm{TCP}_{\mathrm{pop}}$ value (horizontal dash-dotted line), representing the proportion of patients expected to achieve sustained tumor control. The time $t_{1/2}$ (vertical dashed line) indicates the characteristic time at which LC approaches $\mathrm{TCP}_{\mathrm{pop}}$. This corresponds to the definition in Equation (2.35).

2.3 Data Search and Collection

The database *PubMed* was used to identify eligible studies using the following keywords, including tumor site: *local control*, *local control and dose volume*, *stereotactic radiosurgery and local control*. All manuscripts identified in this way were assessed. The selection criteria were that the prescription dose, fractionation and tumor size had to be clearly reported with the corresponding local control after a certain follow-up time. These terms were extracted from all eligible studies for the four tumor sites: *pyriform sinus*, *breast*, *non-small cell lung cancer (NSCLC)* and *brain metastases*.

2.3.1 Dose Estimation

For NSCLC and brain metastases, we looked for trials that used either *conventional fractionation (CF)* or *hypofractionation (HF)*, whereas for pyriform sinus and breast, only conventional fractionation is common.
If the study documented the mean or median dose for CF data, this information was used. In studies where different dose regimens were used, the mean reported dose was calculated. To account for differences in the distribution of patients in different dose regimens, the mean dose was calculated as a weighted average, with the weight proportional to the number of patients or the number of brain metastases in each regimen.

In studies involving HF, it is common practice to express the radiation dose delivered to the tumor margin in terms of isodose lines. An isodose line represents a contour within a treatment plan that connects points receiving the same percentage of the prescribed dose. In this context, the dose prescribed to the tumor margin (minimum dose) typically refers to a specific isodose line (e.g. the 95% isodose), meaning that the margin of the tumor receives 95% of the prescribed total dose. The mean dose was then approximated by averaging the minimum dose (dose at the tumor margin) and the maximum dose. Another common metric used to quantify the uniformity of the radiation dose distribution within the target volume is the *heterogeneity index (HI)*. It is defined as the ratio of the maximum dose in the *planning target volume (PTV)* and the prescription dose in the PTV. A HI larger than one therefore indicates a heterogeneous dose distribution, with some regions receiving a higher dose than prescribed [12]. In studies where only the HI was given, the mean dose was obtained by averaging the prescription dose and the maximum dose obtained from the mean HI.

2.3.2 Volume Estimation

For tumor volumes, the goal was to consistently extract the *mean* tumor volume from each study. When only the *median* volume was reported, the mean of an exponential distribution was estimated using the following relation:

$$V_{mean} = \frac{V_{median}}{\log 2}. \tag{2.36}$$

If only the mean diameter d was provided, the mean tumor volume was calculated assuming the tumor to be spherical:

$$\bar{V} = \frac{4}{3}\pi r^3, \tag{2.37}$$

where r is the radius determined by $r = \frac{d}{2}$. In some studies, only a range of volumes was documented. In these cases, an exponential distribution was applied from Equation (2.29), equating it to the fraction of patients in the specific volume category defined by the range from V_1 to V_2:

$$\int_{V_1}^{V_2} \frac{1}{\bar{V}} e^{-\frac{V}{\bar{V}}}\, dV = \frac{N_{subgroup}}{N_{total}}. \tag{2.38}$$

Computing the integral and rearranging the equation according to $\bar{V}$, we get the required average volume. With this average volume, we can then calculate the average volumes for each subgroup:

$$\bar{V}_{subgroup} = \frac{\int_{V_1}^{V_2} \frac{1}{\bar{V}} e^{-\frac{V}{\bar{V}}} V \, dV}{\int_{V_1}^{V_2} \frac{1}{\bar{V}} e^{-\frac{V}{\bar{V}}} \, dV}, \tag{2.39}$$

where the numerator represents the expected value of V between V_1 and V_2, weighted by the probability density function of the exponential distribution. The denominator serves as a normalization factor. Conversely, if the information on the number of patients in the subgroups is missing, we can insert the mean volume $\bar{V}$ and the total number of patients N_{total} in Equation (2.38) and rearrange it according to $N_{subgroup}$. For NSCLC and pyriform sinus, tumor stage information was sometimes available instead of volume ranges. In such instances, the upper limit of the respective stage was used as the upper boundary for integration, while the lower boundary was defined as the upper limit of the preceding tumor stage. For NSCLC, the reported upper limits of $T_1 = 3cm$ and $T_2 = 7cm$ were used as the maximum diameter, as specified in the ACCJ cancer staging manual [13]. For pyriform sinus the respective ranges for T_1 and T_2 were consistently documented in the studies.

2.3.3 Collection of Local Control Data

Local control, along with its synonyms “freedom from local failure”, “local progression alone,” and “local recurrence-free survival” was collected for several years of follow-up. In instances where these data were not explicitly stated, they were extrapolated from Kaplan-Meier curves using the Web-Plot-Digitizer [14].

2.4 Tumor Sites

Four different tumor sites were studied in this work. For each site, relevant papers were gathered to extract the information necessary for the analysis. In total, five studies for *pyriform sinus* were collected, which are listed in Table 1. For *breast*, only one study was found where the patients were treated exclusively with radiotherapy [15]. The *NSCLC* dataset includes twelve series of conventionally fractionated local studies (Table 4) and eleven sets of hypofractionated studies (Table 5). For *brain metastases*, 22 studies (Table 6) were identified to evaluate the accuracy of the population LC model. Further information on each of the four tumor sites and the corresponding clinical data is provided in the following subsections.

2.4.1 Pyriform Sinus

The pyriform sinus is part of the pharynx, specifically the pear-shaped subsite of the hypopharynx located posterolaterally to either side of the laryngeal opening [16]. Pyriform sinus cancer is strongly associated with risk factors such as smoking and heavy alcohol consumption [17]. Due to its anatomical location, this type of cancer is often diagnosed at advanced stages when the disease has potentially spread to nearby lymph nodes or tissues [17]. For localized pyriform sinus cancer, conventional radiation therapy is the primary treatment approach, often combined with chemotherapy to enhance efficacy. In advanced cases, treatment may also involve surgery. However, in this work, only studies were included in which conventional radiation therapy alone was used for the treatment of pyriform sinus cancer (Table 1).

Table 1 Clinical data on pyriform sinus cancer patients treated with conventional fractionation, detailing mean radiation doses, tumor sizes, local control (LC) rates, follow-up periods in months, and number of patients (pts.). As the follow-up time increases, local control tends to decrease. Smaller volumes and larger doses are associated with improved local control at a given follow-up time.

	Mean dose [Gy]		Tumor size	LC	Follow-up [months]	No. of pts.
	Total	d_f	$\bar{V}$ [cm^3]			
Blanchard	70	2	14.53	0.96	12	107
(2012)[18]	70	2	14.53	0.9	24	107
	70	2	14.53	0.88	36	107
	70	2	14.53	0.85	48	107
	70	2	14.53	0.85	60	107
	70	2	61.42	0.8	12	87
	70	2	61.42	0.74	24	87
	70	2	61.42	0.73	36	87
	70	2	61.42	0.72	48	87
	70	2	61.42	0.61	60	87
Nakajima	70	2	2	0.87	12	24
(2012)[19]	70	2	2	0.87	24	24
	70	2	2	0.87	36	24
	70	2	2	0.87	48	24
	70	2	2	0.87	60	24
	70	2	2	0.87	72	24
	70	2	14.55	0.86	12	79
	70	2	14.55	0.83	24	79
	70	2	14.55	0.83	36	79
	70	2	14.55	0.79	48	79
	70	2	14.55	0.79	60	79
	70	2	14.55	0.71	72	79
Rabbani	74.4	2	2.34	0.92	60	49
(2008)[20]	74.4	2	7.78	0.67	60	6

Continued on next page

Table 1 – continued from previous page

	Mean dose [Gy]		Tumor size	LC	Follow-up [months]	No. of pts.
	Total	d_f	$\bar{V}$ [cm^3]			
Pamejier	70.9	2	3.25	0.89	24	19
(1998)[21]	70.9	2	8	0.25	24	4
Bataini	47.5	2	127.54	0.14	24	14
(1982)[22]	52.5	2	127.54	0.27	24	22
	57.5	2	127.54	0.42	24	31
	62.5	2	127.54	0.43	24	47
	67.5	2	127.54	0.46	24	96
	72.5	2	127.54	0.42	24	59
	77.5	2	127.54	0.43	24	21

2.4.2 Breast

Breast cancer is a type of cancer that originates from the breast tissue, typically arising in the cells of the lobules (glands responsible for milk production) or the ducts (channels that transport milk from the lobules to the nipple) [23]. It is one of the most common cancers diagnosed in women, although it can also occur in men.
Historically, treatment primarily consisted of mastectomy or radiotherapy alone. A mastectomy refers to the surgical removal of one or both breasts. In recent years, treatment strategies have evolved significantly. Lumpectomy, followed by radiotherapy, has largely replaced mastectomy. A lumpectomy involves the surgical removal of only the tumor along with a small margin of surrounding healthy tissue, preserving most of the breast. This procedure is typically followed by radiation therapy to reduce the likelihood of local recurrence [24].
In the study by Arriagada et al. [15], only cases exclusively treated with radiotherapy were considered. The indication for radiotherapy alone was limited to patients with inoperable tumors and those refusing a mastectomy. These patients either had operable tumors, but were unfit for general anesthesia, or had inoperable tumors due to local contraindications to surgery. In the paper, the data is presented in categories based on different dose groups (Table 3) and different volume groups (Table 2). When distinguishing between different dose groups, a constant tumor volume was assumed, corresponding to the cohort's mean tumor volume of 165 cm^3. Similarly, for the volume groups, a constant mean dose of 61.3 Gy was applied.

Table 2 Clinical data on breast cancer patients from the study by Arriagada et al. [15], who were treated with conventional fractionation and received a mean total radiation dose of 61.3 Gy. This table presents detailed information on local control (LC) rates, follow-up periods in months and the number of patients (pts.) within each volume group. As the follow-up time increases, local control tends to decrease within each volume group. Smaller volumes are associated with improved local control at a given follow-up time.

Tumor size $\bar{V}$ [cm^3]	LC	Follow-up [months]	No. of pts.
16.18	0.94	12	55
16.18	0.87	24	55
16.18	0.74	36	55
16.18	0.74	48	55
16.18	0.72	60	55
16.18	0.67	72	55
16.18	0.62	94	55
16.18	0.61	108	55
73	0.82	12	124
73	0.62	24	124
73	0.46	36	124
73	0.4	48	124
73	0.36	60	124
73	0.35	72	124
73	0.29	94	124
73	0.25	108	124
178.59	0.8	12	107
178.59	0.53	24	107
178.59	0.45	36	107
178.59	0.38	48	107
178.59	0.35	60	107
178.59	0.31	72	107
178.59	0.31	94	107
178.59	0.31	108	107
364.32	0.69	12	61
364.32	0.5	24	61
364.32	0.24	36	61
364.32	0.21	48	61
364.32	0.15	60	61
364.32	0.15	72	61
364.32	0.15	94	61
523.6	0.58	12	46
523.6	0.29	24	46

Continued on next page

Table 2 – continued from previous page

Tumor size $\bar{V}$ [cm^3]	LC	Follow-up [months]	No. of pts.
523.6	0.26	36	46
523.6	0.2	48	46
523.6	0.16	60	46

Table 3 Clinical data on breast cancer patients from the study by Arriagada et al. [15], treated using conventional fractionation. This table presents detailed information on local control (LC) rates, follow-up periods in months and the number of patients (pts.) within each dose group, assuming a mean tumor volume of 165 cm^3. As the follow-up time increases, local control tends to decrease within each dose group. Increasing the mean total dose delivered is associated with improved local control at a given follow-up time.

Mean total Dose [Gy]	LC	Follow-up [months]	No. of pts.
35	0.47	12	23
35	0.2	24	23
45	0.63	12	103
45	0.36	24	103
45	0.17	36	103
45	0.13	48	103
45	0.11	60	103
55	0.7	12	80
55	0.51	24	80
55	0.36	36	80
55	0.35	48	80
55	0.29	60	80
55	0.27	72	80
55	0.22	94	80
55	0.22	108	80
55	0.2	120	80
65	0.88	12	165
65	0.6	24	165
65	0.39	36	165
65	0.3	48	165
65	0.3	60	165
75	0.92	12	104
75	0.75	24	104
75	0.67	36	104
75	0.64	48	104
75	0.62	60	104

Continued on next page

Table 3 – continued from previous page

Mean total Dose [Gy]	LC	Follow-up [months]	No. of pts.
75	0.62	72	104
75	0.54	94	104
75	0.53	108	104
85	0.95	12	53
85	0.9	24	53
85	0.83	36	53
85	0.66	48	53
85	0.65	60	53
85	0.64	72	53
85	0.59	94	53
85	0.59	108	53

2.4.3 NSCLC

Non-small cell lung cancer is the second most common cancer in the world. In the past, the usual treatment for patients with early-stage NSCLC that could not be surgically removed was conventional radiation therapy. This method typically consists of doses of 2 – 3 Gy in each session, adding up to about 54 – 60 Gy in total. However, the long-term results from this approach have not been very effective, with local control rates around 30-70% and overall survival rates between 15-30% [25].

Recent improvements in imaging technology and radiation treatment planning have made it possible to deliver "ablative doses", meaning highly destructive levels of radiation. This method is known as stereotactic body radiation therapy. It allows doctors to give higher doses of radiation, usually about 18 – 20 Gy over three sessions, directly to small tumors with great precision [25].

In this work data from both conventional fractionated treatments (Table 4) and hypofractionated treatments (Table 5) are analyzed for NSCLC, allowing to compare outcomes across different fractionation approaches.

Table 4 Clinical data on non-small cell lung cancer patients treated with conventional fractionation, detailing mean radiation doses, tumor sizes, local control (LC) rates, follow-up periods in months, and number of patients (pts.). As the follow-up time increases, the local control tends to decrease.

	Mean dose [Gy]		Tumor size	LC	Follow-up [months]	No. of pts.
	Total	d_f	$\bar{V}$ [cm^3]			
Bradley	70	2	2.02	0.83	24	16

Continued on next page

Table 4 – continued from previous page

	Mean dose [Gy]		Tumor size	LC	Follow-up [months]	No. of pts.
	Total	d_f	$\bar{V}$ [cm^3]			
(2003)[26]	70	2	8.74	0.62	24	19
	70	2	29.62	0.5	24	15
Bradley	70	2	246.60	0.478	12	45
(2002)[27]	70	2	246.60	0.321	24	45
	70	2	246.60	0.320	36	45
	70	2	140.70	0.768	12	31
	70	2	140.70	0.578	24	31
	70	2	140.70	0.580	36	31
	70	2	89.50	0.710	12	33
	70	2	89.50	0.520	24	33
	70	2	89.50	0.520	36	33
	70	2	89.50	0.520	48	33
	70	2	50.37	0.807	12	23
	70	2	50.37	0.648	24	23
	70	2	50.37	0.427	36	23
	70	2	16.32	0.890	12	41
	70	2	16.32	0.791	24	41
	70	2	16.32	0.791	36	41
	70	2	16.32	0.689	48	41
Sandler	60	2	136.50	0.297	12	9
(1990)[28]	60	2	136.50	0.297	24	9
	60	2	37.55	0.615	12	41
	60	2	37.55	0.447	24	41
	60	2	37.55	0.371	36	41
	60	2	6.36	0.766	12	25
	60	2	6.36	0.624	24	25
	60	2	6.36	0.477	36	25
	60	2	6.36	0.476	48	25
Willner	59.9	2	317.16	0.196	12	20
(2002)[29]	59.9	2	317.16	0.098	24	20
	59.9	2	110.36	0.492	12	65
	59.9	2	110.36	0.226	24	65
	59.9	2	110.36	0.227	36	65
	59.9	2	23.32	0.602	12	107
	59.9	2	23.32	0.526	24	107
	59.9	2	23.32	0.406	36	107
Bogart	70	2.5	5.67	0.83	36	31
(2005)[30]						
Hayakawa	67	2	65.38	0.94	12	36
(1999)[31]	67	2	65.38	0.785	24	36
	67	2	65.38	0.72	36	36
	67	2	65.38	0.72	48	36
	67	2	65.38	0.72	60	36

Continued on next page

Table 4 – continued from previous page

	Mean dose [Gy]		Tumor size	LC	Follow-up [months]	No. of pts.
	Total	d_f	$\bar{V}$ [cm^3]			
Cheung	48	4	38.79	0.835	12	33
(2002)[32]	48	4	38.79	0.7	24	33
	48	4	38.79	0.62	36	33
Langendijk	70	2	17.68	0.87	12	46
(2002)[33]	70	2	17.68	0.71	24	46
	70	2	17.68	0.5	36	46
Lagerwaard	66	2	16.61	0.85	12	113
(2002)[34]	66	2	16.61	0.57	24	113
	66	2	16.61	0.43	36	113
	66	2	16.61	0.43	48	113
Rosenzweig	70.2	1.8	5.19	0.75	12	32
(2001)[35]	70.2	1.8	5.19	0.43	24	32
	70.2	1.8	5.19	0.43	36	32
	70.2	1.8	5.19	0.43	48	32
	70.2	1.8	5.19	0.43	60	32
	70.2	1.8	5.19	0.43	72	32
Shirata	60	4	9.41	1	12	7
(2012)[36]	60	4	9.41	0.57	24	7
	60	4	9.41	0.57	36	7
	60	4	9.41	0.57	48	7
	60	4	9.41	0.57	60	7
Martel	75.5	2	221	0.55	24	41
(1997)[37]	75.5	2	221	0.37	60	41
	66	2	221	0.47	24	35
	66	2	221	0.32	60	35

Table 5 Clinical data on non-small cell lung cancer patients treated with hypofractionation, detailing mean radiation doses, tumor sizes, local control (LC) rates, follow-up periods in months, and number of patients (pts.). As the follow-up time increases, the local control tends to decrease.

	Mean dose [Gy]		Tumor size	LC	Follow-up [months]	No. of pts.
	Total	d_f	$\bar{V}$ [cm^3]			
Fritz	27	27	13.52	1	12	40
(2008)[38]	27	27	13.52	0.96	24	40
	27	27	13.52	0.81	36	40
Baummann	56.1	18.7	16	0.92	36	57
(2009)[39]						
Stephans	69.3	23.1	6.24	1	12	38
(2009)[40]	69.3	23.1	6.24	1	18	38
	52.8	10.56	4.85	0.982	12	56
	52.8	10.56	4.85	0.953	24	56
	52.8	10.56	4.85	0.953	36	56
Crabtree	59.7	19.9	5.49	0.964	12	57
(2009)[41]	59.9	19.2	5.49	0.884	24	57
	59.7	19.9	5.49	0.884	36	57
	59.7	19.9	5.49	0.884	48	57
	59.7	19.9	5.49	0.884	60	57
	59.7	19.9	24.01	0.94	12	25
	59.7	19.9	24.01	0.94	24	25
	59.7	19.9	24.01	0.94	36	25
	59.7	19.9	24.01	0.94	48	25
	59.7	19.9	24.01	0.94	60	
Timmer-	59.9	19.9	8.8	0.976	36	55
mann						
(2010)[42]						
Videtic	53.8	10.76	4	0.931	36	22
(2010)[43]	53.8	10.76	18.32	1	36	6
Shibamoto	44	11	1.33	1	12	4
(2012)[44]	44	11	1.33	1	24	4
	44	11	1.33	1	36	4
	48	12	6.25	0.95	12	124
	48	12	6.25	0.9	24	124
	48	12	6.25	0.86	36	124
	48	12	6.25	0.86	48	124
	48	12	6.25	0.86	60	124
	48	12	6.25	0.86	72	124
	52	13	21.2	0.89	12	52
	52	13	21.2	0.8	24	52
	52	13	21.2	0.73	36	52
	52	13	21.2	0.73	48	52
	52	13	21.2	0.73	60	52
	52	13	21.2	0.73	72	52

Continued on next page

Table 5 – continued from previous page

	Mean dose [Gy]		Tumor size	LC	Follow-up [months]	No. of pts.
	Total	d_f	$\bar{V}$ [cm^3]			
Shirata	48	12	9.41	1	12	45
(2012)[36]	48	12	9.41	1	24	45
	48	12	9.41	1	36	45
	48	12	9.41	1	48	45
	48	12	9.41	1	60	45
	60	7.5	9.41	1	12	29
	60	7.5	9.41	0.95	24	29
	60	7.5	9.41	0.82	36	29
	60	7.5	9.41	0.82	48	29
	60	7.5	9.41	0.82	60	29
Takaeda	56.3	11.26	7.97	0.927	12	62
(2013)[45]	56.3	11.26	7.97	0.876	24	62
	56.3	11.26	7.97	0.836	36	62
Hamaji	48	12	8.18	0.96	12	99
(2015)[46]	48	12	8.18	0.8	24	99
	48	12	8.18	0.76	36	99
	48	12	8.18	0.74	48	99
	48	12	8.18	0.72	60	99
	48	12	8.18	0.68	72	99
	48	12	8.18	0.68	84	99
	48	12	8.18	0.68	96	99
	48	12	8.18	0.34	108	99
Rwigema	68.9	22.97	6.94	1	12	46
(2014)[47]	68.9	22.97	6.94	0.955	24	46
	68.9	22.97	6.94	0.955	36	46

2.4.4 Brain Metastases

Radiation therapy (RT) plays an essential role in the management of brain metastases. Conventional radiation treatment fields may be used to deliver radiation to the whole brain. However, numerous studies have demonstrated a relationship between large field brain RT and both neuropsychological sequelae and deterioration in quality of life [48]. Thus, the use of stereotactic radiosurgery or fractionated stereotactic radiation therapy to treat brain metastases, without *whole-brain radiation therapy (WBRT)*, has been increasing. Consequently, WBRT studies were excluded from the analysis. Some of the studies include patients treated with a *Gamma Knife (GK)*, whereas other studies focused on those treated with linear accelerator (LINAC)-based systems.

Table 6 Clinical data on brain metastases patients, detailing mean radiation doses, tumor sizes, local control (LC) rates, follow-up periods in months, and number of brain metastases (BM). As the follow-up time increases, the local control tends to decrease. Smaller tumors allow for more precise radiation delivery, enabling the use of higher doses per fraction while minimizing damage to surrounding healthy tissue.

	Mean dose [Gy]		Tumor size	LC	Follow-up [months]	No. of BM
	Total	d_f	$\bar{V}$ [cm^3]			
Baschnagel (2013)[49]	27	27	0.74	0.99	6	337
	27	27	0.74	0.97	12	337
	27	27	0.74	0.93	24	337
	27	27	0.74	0.93	36	337
	27	27	3.25	0.9	6	86
	27	27	3.25	0.75	12	86
	27	27	3.25	0.69	24	86
	27	27	3.25	0.69	36	86
Ko (2020)[50]	24	24	0.33	0.96	6	126
	24	24	0.33	0.94	12	126
	24	24	0.33	0.68	24	126
	24	24	0.33	0.68	36	126
	24	24	0.33	0.55	48	126
	24	24	1.45	0.75	6	15
	24	24	1.45	0.61	12	15
	24	24	1.45	0.31	24	15
	24	24	1.45	0.2	36	15
Higuchi (2009)[51]	30	10	17.6	0.9	6	46
	30	10	17.6	0.76	12	46
	30	10	17.6	0.65	24	46
Lutterbach (2003)[52]	20.25	20.25	7	0.93	6	103
	20.25	20.25	7	0.91	12	103
	20.25	20.25	7	0.79	24	103
Saitoh (2010)[53]	41.15	13.7	1.3	0.86	12	24
Aoyama (2003)[54]	38	9.5	1.39	0.96	6	72
	38	9.5	1.39	0.96	12	72
	38	9.5	1.39	0.84	24	72
	38	9.5	9.65	0.71	6	68
	38	9.5	9.65	0.59	12	68
	38	9.5	9.65	0.48	24	68
Lindvall (2005)[55]	42.2	8.44	6.5	0.84	12	60
Tokuuye (1998)[56]	42	6	8.18	0.91	12	95
Jani (2015)[57]	28.18	28.18	0.97	0.97	6	216
	28.18	28.18	0.97	0.9	12	216
	28.18	28.18	0.97	0.83	24	216
	25.36	25.36	5.24	0.94	6	110

Continued on next page

Table 6 – continued from previous page

	Mean dose [Gy]		Tumor size	LC	Follow-up [months]	No. of BM
	Total	d_f	$\bar{V}$ [cm^3]			
	25.36	25.36	5.24	0.79	12	110
	25.36	25.36	5.24	0.65	24	110
	22.55	22.55	15.14	0.91	6	47
	22.55	22.55	15.14	0.71	12	47
	22.55	22.55	15.14	0.53	24	47
Minniti	29.38	9.79	25.25	0.93	12	101
(2013)[58]	29.38	9.79	25.25	0.84	24	101
Shehata	20	20	0.43	0.93	6	228
(2004)[59]	20	20	0.43	0.77	12	228
	20	20	0.43	0.67	24	228
Feuvret	23.1	7.7	29.4	1	12	12
(2014)[60]	23.1	7.7	29.4	0.64	24	12
	14	14	15.6	0.58	12	24
	14	14	15.6	0.48	24	24
Murai	16.5	16.5	3.69	0.98	6	40
(2014)[61]	16.5	16.5	3.69	0.93	12	40
	16.5	16.5	3.69	0.93	24	40
	25.71	8.57	11.24	0.88	6	29
	25.71	8.57	11.24	0.86	12	29
	25.71	8.57	11.24	0.76	24	29
	27.3	9.1	22.39	0.85	6	20
	27.3	9.1	22.39	0.8	12	20
	27.3	9.1	22.39	0.68	24	20
	28.27	5.654	47.4	0.69	6	13
	28.27	5.654	47.4	0.46	12	13
Nagai	31.14	7.785	0.12	0.98	6	43
(2014)[12]	31.14	7.785	0.12	0.98	12	43
	31.14	7.785	0.12	0.72	24	43
	31.14	7.785	0.6	0.86	6	42
	31.14	7.785	0.6	0.82	12	42
	31.14	7.785	0.6	0.75	24	42
	31.14	7.785	2.9	0.93	6	43
	31.14	7.785	2.9	0.93	12	43
	31.14	7.785	2.9	0.93	24	43
Zairi	23.41	23.41	2.47	0.92	12	115
(2014)[62]	23.41	23.41	2.47	0.86	24	115
Eliott	30	30	0.49	0.96	6	255
(2011)[63]	30	30	0.49	0.93	12	255
	30	30	0.49	0.89	24	255
	30	30	0.49	0.88	36	255
Matsuo	27	4.5	4.49	0.8	6	30
(1999)[64]	27	4.5	4.49	0.58	12	30
	27	4.5	4.49	0.47	24	30

Continued on next page

Table 6 – continued from previous page

	Mean dose [Gy]		Tumor size	LC	Follow-up [months]	No. of BM
	Total	d_f	$\bar{V}$ [cm^3]			
	35	5	4.15	1	6	30
	35	5	4.15	0.9	12	30
	35	5	4.15	0.9	24	30
	35	5	4.15	0.9	36	30
Aoyama	29.38	7.345	6.7	0.62	6	22
(1999)[54]	29.38	7.345	6.7	0.52	12	22
	40.8	10.2	6.7	0.89	6	118
	40.8	10.2	6.7	0.86	12	118
Blongien	20.25	20.25	0.539	0.85	13.7	173
(2010)[65]						
Inoue	42.225	8.445	12.6	0.98	6	185
(2014)[66]	42.225	8.445	12.6	0.98	12	185
	42.225	8.445	12.6	0.79	24	185
	42.225	8.445	12.6	0.52	36	185
Minniti	24.49	8.16	17.75	0.98	6	47
(2016)[67]	24.49	8.16	17.75	0.7	12	47
	24.49	8.16	17.75	0.6	24	47
Minniti	33.735	11.245	10.1	0.99	6	171
(2014)[68]	33.735	11.245	10.1	0.88	12	171
	33.735	11.245	10.1	0.72	24	171
	33.735	11.245	10.1	0.65	36	171

2.5 Optimizing Model Parameters with Maximum Likelihood Method

The estimation of the model parameters was performed using the maximum likelihood method, which allows us to estimate the parameters of the model by maximizing the likelihood of observing local control given the parameters.

This method involves a two-step approach of parameter fitting for both the LQ and the TE model. In the first step, the time-dependent expression for local control (Equation (2.34)) is fitted for the constant average tumor control probability ($\mathrm{TCP}_{\mathrm{pop}}$) and the local control rate λ. In the second step, the fit of Equation (2.34) is refined by incorporating the model-specific tumor control probability function at the end of Section 2.2, which depends on additional parameters. For the LQ model, these parameters are α, σ_α and β, while for the TE model, they are p, σ_p and q. The λ obtained from the initial fit is used as a fixed input, allowing the remaining parameters to be optimized for each model.

Using the likelihood function, the probability of observing the data given the current model parameters is calculated. LC is binomially distributed since it involves a fixed number of patients (trials), each of whom can experience one of two outcomes: success (local control) or failure (tumor recurrence). A binomial distribution is therefore used

to construct the likelihood function $\mathcal{L}_p$ for parameter optimization. This function is expressed as:

$$\mathcal{L}_p = \prod_{i=1}^{n} \binom{M_i}{K_i} \mathrm{LC}_i^{K_i} \left(1 - \mathrm{LC}_i\right)^{M_i - K_i}, \tag{2.40}$$

where:

- M_i is the total number of patients in study group i,
- K_i is the number of successful tumor control cases in group i,
- LC_i is the predicted LC value for group i.

To avoid numerical issues with very small probabilities, the log-likelihood is used, defined as:

$$\log \mathcal{L}_p = \sum_{i=1}^{n} \left(K_i \log(\mathrm{LC}_i) + (M_i - K_i) \log(1 - \mathrm{LC}_i) + \log \binom{M_i}{K_i} \right). \tag{2.41}$$

In order to maximize the log-likelihood and determine the best-fitting parameters, a grid search algorithm is employed. This iterative process refines the search area for each parameter in the following steps:

1. **Initial parameter ranges:** Initial biologically plausible parameter ranges, detailed in Appendix A.1, are defined. For each iteration, a grid of possible values within these ranges is generated.
2. **Log-likelihood calculation:** For each combination of parameters in the grid, the log-likelihood is calculated using the binomial log-likelihood function (2.41).
3. **Refinement:** After each iteration, the parameter ranges are refined around the values that maximize the objective function. The ranges are updated by shrinking them by 10% of their current size around the best parameters found.
4. **Convergence:** The process is repeated until the objective function converges to the maximum value that yields the optimal parameters.

The variation parameters σ_α and σ_p were constrained to be less than or equal to α and p, respectively. The confidence intervals for the parameters were determined using a bootstrapping approach with 1000 resampled datasets. For each bootstrap sample, differential evolution was employed to estimate the optimal parameter values for each dataset. After obtaining the parameter estimates from all 1000 bootstrap samples, the confidence interval is calculated by taking the appropriate percentiles of

the parameter distributions. The significance of the fitted parameters was assessed through a Wald test at a significance level of 0.05. All statistical analyses were implemented using Python 3.10. The final parameter estimates are presented in Chapter 3 and summarized in Table A4 in the Appendix A.2. The maximum log-likelihood values obtained from the maximum-likelihood estimation are provided in Section 3.5.

2.6 Visualization

After determining the relevant parameters, they are inserted into the models, and the results are plotted alongside the data. Tumor control probability for each survival model is illustrated by plotting it once as a function of dose and once as a function of tumor volume. To calculate $\mathrm{TCP}_{\mathrm{pop}}$, Equation (2.34) is used in combination with the local control data at the corresponding follow-up times and the fitted value of λ. In each plot, the data is categorized by applying a threshold, setting either a volume or dose cut-off and sorting data according to that threshold. Data points below the threshold are displayed in black, while those above it are shown in green. The models for each category are visualized by inserting the mean value for that category into the models, with the results plotted in the corresponding color.
In the representation of local control (Equation (2.34)) as a function of follow-up time, data is similarly categorized by volume or dose. Unlike the previous plots, both a fixed volume and a fixed dose value are required as inputs to the model. This is achieved by first sorting the data based on a chosen threshold, either volume or dose, which creates two categories. For each category, the mean volume and mean dose are calculated and used as fixed inputs in the models.
To improve the clarity of the plots, data points sharing similar or identical x-axis positions are grouped into bins. For each bin, the average TCP or LC value is calculated from all corresponding data points, and only this averaged value is displayed. This approach provides a cleaner, more interpretable visual representation of the data trends.
To calculate the uncertainties associated with each average TCP or LC, we start by determining the standard deviation SD for each category:

$$\mathrm{SD} = \sqrt{\frac{1}{n-1}\sum_{i=1}^{n}(x_i - \bar{x})^2}, \tag{2.42}$$

where

- n is the number of values in the category,
- x_i represents each individual value in the category,

– $\bar{x}$ is the mean of the values in the category calculated as $\bar{x} = \frac{1}{n}\sum_{i=1}^{n} x_i$.

Once the standard deviation SD is known, the standard error of the mean SE can be calculated by dividing SD by the square root of the number of data points n in the category:

$$\mathrm{SE} = \frac{\mathrm{SD}}{\sqrt{n}}. \tag{2.43}$$

With the standard error of the mean SE we can effectively display this uncertainty as error bars in the plots.

For direct comparison, the breast data is presented in a format consistent with the study by Arriagada et al. [15]. In Table 3, where the volume is held as constant with a mean value of 165 cm^3, the local control data is categorized into six different groups based on dose. In Table 2, where the dose is constant with a mean value of 61.3 Gy, the local control data is sorted into five groups based on tumor size. In both plots, each group is represented by a distinct color. Local control is then plotted as a function of follow-up time for each group, using the mean value of each group as input to the models.

To enable consistent comparisons between conventional fractionation and hypofractionation studies, the total dose has been standardized to an equivalent dose of 2 Gy per fraction for all NSCLC plots.

In the plots for brain metastases, the doses to a single-fraction equivalent dose has been converted by inserting the fitted parameters into Equation (2.8) for the LQ model and Equation (2.26) for the TE model.

2.7 Radiation Necrosis

As discussed in Section 2.4.4, stereotactic radiosurgery or fractionated stereotactic radiation therapy is the standard treatment for patients with brain metastases. However, these therapies are not without risks, as late toxicities have been documented after SRS, with *radiation necrosis (RN)* being the most common complication. Studies indicate that RN can develop in up to 50% of treated lesions, with a significant percentage of these cases showing clinical symptoms [69].

Radiation necrosis is defined as the unplanned death of cells and tissues due to cumulative radiation damage. Unlike apoptosis, a regulated and controlled cell death, necrosis is an uncontrolled process triggered by DNA damage, mitochondrial dysfunction, and vascular injury within the irradiated brain region [70]. The damaged cells spill their contents into the surrounding tissue and release inflammatory molecules. This leads to edema (swelling) and damage to neighboring cells, sometimes resulting in additional neurological deficits [71].

RN usually manifests within six months but it can also occur years after standard

RT. The diagnosis of RN is based on a combination of clinical and imaging findings. On radiological imaging, it is often challenging to clearly distinguish between tumor recurrence and necrosis. Other clinical investigations, such as biopsy or advanced imaging techniques like the combination of MRI and PET, are necessary to confirm the diagnosis of RN [72]. Once RN is detected, we further distinguish symptomatic and asymptomatic RN. This work focuses exclusively on symptomatic RN, as this form significantly impacts patients' quality of life and requires clinical management.

2.7.1 Models of Symptomatic Radiation Necrosis Probability

To quantify the probability of *symptomatic radiation necrosis (SRN)*, we use two simple models: a logistic model and its logarithmic form.
The logistic model [73], here referred to as the exponential model, is defined as:

$$P_{\mathrm{SRN}} = \frac{\exp\left(4\gamma_{50}\left(\frac{\mathrm{Vx}}{\mathrm{Vx}_{50}} - 1\right)\right)}{1 + \exp\left(4\gamma_{50}\left(\frac{\mathrm{Vx}}{\mathrm{Vx}_{50}} - 1\right)\right)} \tag{2.44}$$

and its logarithmic form is:

$$P_{\mathrm{SRN}} = \frac{1}{1 + \left(\frac{\mathrm{Vx}_{50}}{\mathrm{Vx}}\right)^{4\gamma_{50}}}\,. \tag{2.45}$$

In these equations Vx_{50} is the volume corresponding to 50% risk of symptomatic radiation necrosis, and γ_{50} is the slope of the logistic function at that point. Vx is the volume of brain tissue irradiated by x Gy. Numerous studies indicate that the radiosurgical volume of brain tissue irradiated by 12 Gy (V12) is the most significant predictor of symptomatic radiation necrosis [74][75][69][76]. Therefore, we set x = 12 Gy to accurately estimate the risk of SRN in treated patients. In studies where the dose differs from 12 Gy, we convert Vx to V12 as follows [74]:

$$\mathrm{V12} = \mathrm{Vx}\left(\frac{12}{d_s}\right)^{s}, \tag{2.46}$$

where $s = 1.15$, determined through the analysis of LINAC-based data with spherical target volumes. In their work, plotting these target volumes against the corresponding doses on a double-logarithmic plot allowed them to determine the slope s as a scaling factor. In this thesis, the slope $s = 1.15$ is applied universally across all treatment machines. For trials where patients were treated with fractionated stereotactic radiosurgery, we need to calculate the single-fraction equivalent dose d_s, i.e. the single dose that yields the same biological effect as a multi-fraction treatment. This can be done using the Equation (2.8) derived from the LQ model, applying an $\frac{\alpha}{\beta}$ ratio of 2, which is typical for healthy brain tissue [73]. Alternatively, we can use Equation (2.26)

derived from the TE model, where we set $p = 0.05$ and $q = 0.25$. The value of p was obtained by fitting the *normal tissue complication probability (NTCP)* model proposed by Zaider et al. [77] to brain necrosis complication data from Emami et al. [78]. The parameter q was then calculated using Equation (2.20), with the fitted p value and an $\frac{\alpha}{\beta}$ ratio of 2.

To estimate the parameters Vx_{50} and γ_{50} for both, single- and multi-fraction treatments, we fit each P_{SRN} model separately: once to the single-fraction data in Table 7 and once to the multi-fraction data in Table 8. This separate fitting is necessary because the logistic models we consider ((2.44), (2.45)) do not incorporate an explicit dependence on fractionation. Therefore we will obtain different parameters for the two datasets. However, the calculation of V12 (Equation (2.46)), which serves as an input to the logistic models, does depend on the dose per fraction and the number of fractions.

The data on SRN were primarily taken from the comprehensive review by Milano et al. [73]. In addition, supplementary data were extracted from one study focusing on SRN after a single-fraction treatment [79] and one after a multi-fraction treatment [80].

The fitting was performed using the maximum likelihood method, which was described in detail in Section 2.5 and adapted to P_{SRN} by replacing LC with P_{SRN} in Equation (2.41). Confidence intervals for the fitted parameters were obtained using bootstrapping with 1000 samples, providing 95% confidence intervals for the estimates. The significance of the parameters was assessed through a Wald test at a significance level of 0.05. The result of the parameter fitting and the fitted curves are presented in Chapter 3. A summary of the estimated parameters can be found in Appendix A.2.

Table 7 Clinical data on single-fraction treatment induced symptomatic radiation necrosis, detailing mean single-fraction doses (d_s), brain volumes receiving 12 Gy (V12), symptomatic radiation necrosis probabilities (P_{SRN}) and number of treated brain metastases (BM). The data show that the probability of SRN increases with increasing V12.

	d_s [Gy]	V12 [cm^3]	P_{SRN}	No. of BM
Sneed	12	0.34	0.0028	707
(2015)[81]	12	1.26	0.01	531
	12	2.58	0.06	177
	12	5.16	0.11	177
	12	21.42	0.11	177
Korytko	12	2.5	0.23	75
(2006)[75]	12	7.5	0.33	12
	12	12.5	0.56	7
	12	22	0.54	11
Minniti	12	8.5	0.1	310

Continued on next page

Table 7 – continued from previous page

	d_s [Gy]	V12 [cm^3]	P_{SRN}	No. of BM
(2011)[69]				
Blonigen	12	7.85	0.1	173
(2010)[65]				
Ohtakara	12	4.074	0.086	131
(2012)[76]				
Lehrer	12	5	0.017	251
(2023)[79]	12	15	0.065	144

Table 8 Clinical data on multiple-fraction treatment induced symptomatic radiation necrosis, detailing number of fractions (n), doses per fraction (d_f), brain volumes receiving x Gy (Vx), symptomatic radiation necrosis probabilities (P_{SRN}) and number of treated brain metastases (BM).

	n	d_f [Gy]	Vx [cm^3]	P_{SRN}	No. of BM
Dore	3	7	10	0.072	97
(2017)[82]					
Inoue	3	7.7	4.7	0	124
(2013)[83]	3	7.7	8.5	0.0857	35
Inoue	5	5.76	4.9	0	69
(2014)[66]	5	5.76	10.4	0.125	16
Upadhyay	3	6.6	2.5	0.009	1080
(2023)[80]	3	7.6	2.5	0.018	1324
	3	6.6	7.5	0.031	617
	3	7.6	7.5	0.033	627
	3	6.6	12.5	0.039	350
	3	7.6	12.5	0.044	297
	3	6.6	17.5	0.046	199
	3	7.6	17.5	0.052	141
	3	6.6	22.5	0.054	272
	3	7.6	22.5	0.06	129

2.8 Complication-free Tumor Control

Achieving tumor control in patients with brain metastases does not necessarily mean that they are in good health. As discussed in the previous section, late toxicities such as radiation necrosis following hypofractionated treatments can significantly impact patients' quality of life. The effectiveness of a given dose distribution can be assessed by weighing its benefits in terms of tumor control against its drawbacks, including the risk of symptomatic radiation necrosis. This balance is quantified by the *complication-free tumor control probability*, which represents the probability of achieving effective tumor control with minimal occurrence of radiation-induced symptomatic necrosis. Assuming that $\mathrm{TCP}_{\mathrm{pop}}$ and P_{SRN} are independent, the complication-free tumor control probability is defined as [84]:

$$\mathrm{TCP}_{\mathrm{complication-free}} = \mathrm{TCP}_{\mathrm{pop}} \left(1 - P_{\mathrm{SRN}}\right). \tag{2.47}$$

Zhao et al. [74] showed a linear relationship between V12 and the tumor volume, given by:

$$\mathrm{V12} = 1.63 \times \bar{V} + 1.38. \tag{2.48}$$

We incorporate this relationship into the P_{SRN} models ((2.44), (2.45)), allowing them to be expressed as a function of tumor volume. Relating V12 directly to the tumor volume, rather than the prescription isodose volume, offers a significant advantage: once the tumor volume is contoured, the probability of radiation necrosis can be calculated. If the calculated RN risk is too high, alternative treatment options can be considered. Inserting the parameters obtained from the individual fits of the TCP and P_{SRN} models, we plot the complication-free TCP as a function of the tumor volume for different fractionation schedules. For multi-fraction schedules, the parameters obtained from the fit to multi-fraction treatment data are applied, whereas for single-fraction schedules, the parameters obtained from the fit to single-fraction treatment data are inserted into the P_{SRN} models. The plots can be found in Chapter 3.

3 Results

In this chapter, we present the results of the model fitting and its analysis. First, we list the parameters obtained by fitting the TCP models for four tumor sites: *pyriform sinus*, *breast*, *NSCLC* and *brain metastases*. This fitting process was conducted in two steps and the resulting parameters, along with their corresponding 95% confidence intervals, are summarized in Table 9 to 14 below. The confidence intervals of the calculated α/β ratio and q were derived using Gaussian error propagation, as explained in Appendix A.4.

For pyriform sinus, NSCLC and brain metastases, plots of the predicted $\mathrm{TCP}_{\mathrm{pop}}$ as a function for both dose and tumor volume are provided. These plots employ Equation (2.34), which expresses $\mathrm{TCP}_{\mathrm{pop}}$ in terms of the local control data at corresponding follow-up times. For NSCLC, the total dose was standardized to EQD2 using Equation (2.6), enabling comparison between CF and HF schedules. For brain metastases, the total dose was converted to a single-fraction equivalent dose using Equation (2.8) for the LQ model and Equation (2.26) for the TE model. For each of these three tumor sites, an additional graph is included to illustrate how LC evolves over follow-up time, highlighting variations of dose levels and tumor volumes.

In the case of breast, two datasets were analyzed independently: one grouped by tumor volume and the other one by dose. For each dataset, local control outcomes are plotted as a function of follow-up time, categorized into five tumor size groups or six dose groups, respectively. The parameters obtained from fitting the dose dataset are used to estimate the residual microscopic tumor volume after surgery. This tumor volume is then used to predict TCP outcomes for typical adjuvant RT regimes. These predictions are presented and discussed in Chapter 4.

Subsequently, the fitting results for the symptomatic radiation necrosis (P_{SRN}) models are shown, specifically for both single-fraction and multi-fraction treatments. Finally, the complication-free tumor control probability is displayed as a function of tumor volume for different fractionation schedules across all models.

3.1 Pyriform Sinus

Table 9 Summary of LQ and TE model parameters for pyriform sinus. The table lists the estimated values for each parameter, along with their 95% confidence intervals (CI). Statistical significance levels are indicated based on the p_{wald} values. Parameters marked with a star (*) correspond to the TE model, where q was obtained by Equation (2.20) using the low-dose approximation. The CI of the calculated α/β ratio and q were derived using Gaussian error propagation.

Parameter [unit]	Value [95% CI]	p_{wald}
TCP_{pop}	$0.74\ [0.68, 0.79]$	< 0.01
λ [months^{-1}]	$0.10\ [0.06, 0.3]$	$= 0.124$
α [Gy^{-1}]	$0.15\ [0.14, 0.35]$	< 0.05
σ_α [Gy^{-1}]	$0.09\ [0.06, 0.19]$	< 0.01
β [Gy^{-2}]	$0.09\ [0.0, 0.1]$	< 0.01
α/β [Gy]	$1.64\ [0.09, 3.19]$	
p [Gy^{-1}]	$0.32\ [0.30, 0.37]$	< 0.01
σ_p [Gy^{-1}]	$0.09\ [0.06, 0.17]$	< 0.01
q [Gy^{-1}]	$0.03\ [0.01, 0.1]$	$= 0.198$
p^* [Gy^{-1}]	$0.16\ [0.15, 0.2]$	< 0.01
σ_p^* [Gy^{-1}]	$0.09\ [0.05, 0.18]$	< 0.01
q^* [Gy^{-1}]	$0.52\ [0.3, 0.74]$	

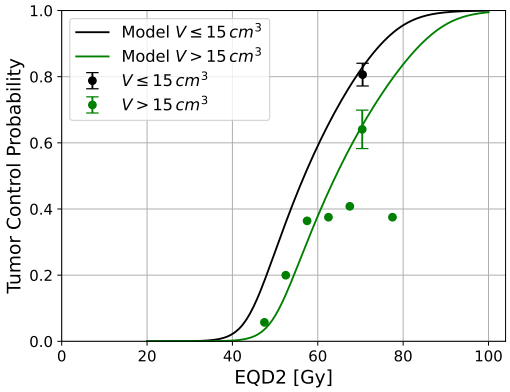

(a) LQ model

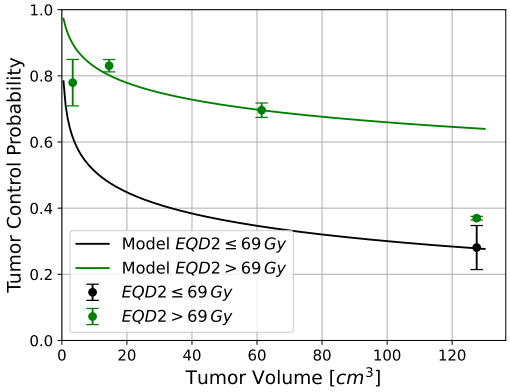

(b) LQ model

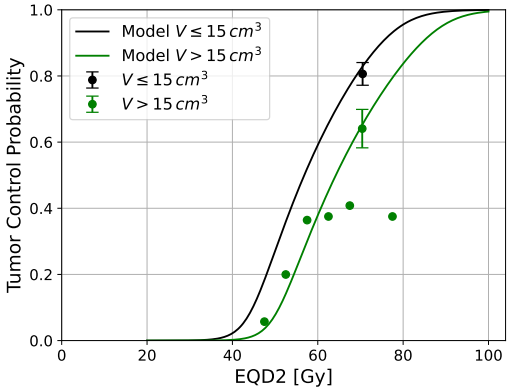

(c) TE model

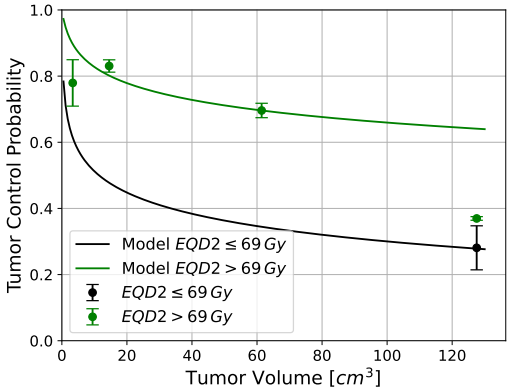

(d) TE model

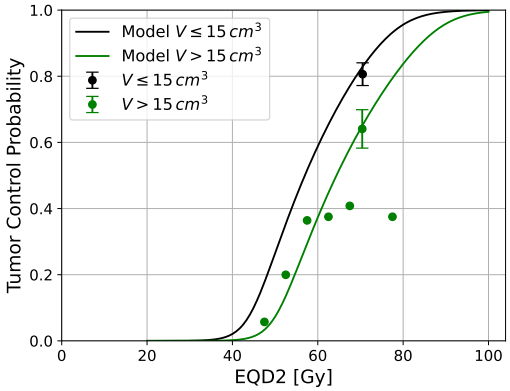

(e) TE model*

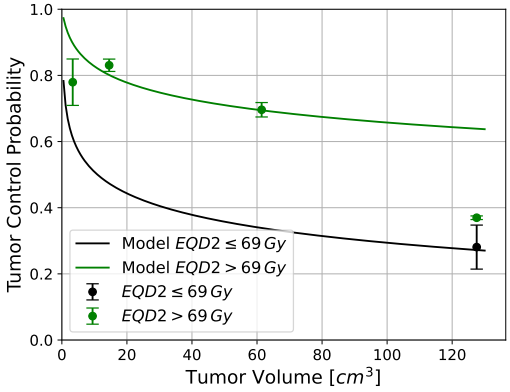

(f) TE model*

Figure 4 Tumor control probability as a function of dose and tumor volume for pyriform sinus across all models. The TE model marked with a star (*) correspond to the variant, where the q value was estimated using the low-dose approximation. The left panel shows tumor control probability as a function of dose, while the right panel shows tumor control probability as a function of tumor volume. The TCP model (solid line) is depicted based on the average total dose and tumor volume in each category and the found parameters from the fit to the complete data set. Error bars represent the standard error of the mean TCP for each group at the respective dose/volume value.

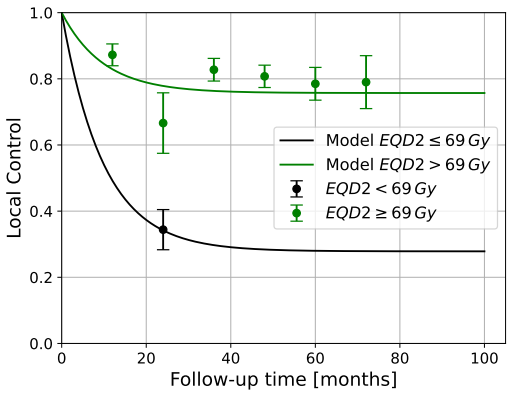

(a) LQ model

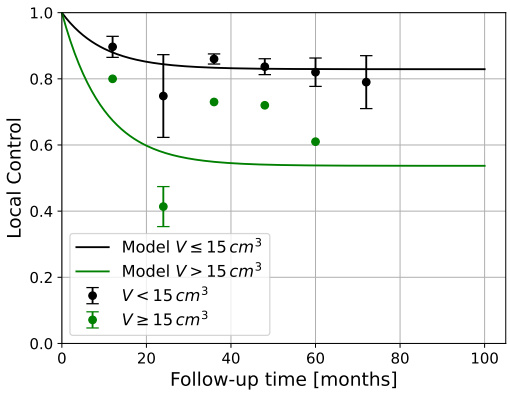

(b) LQ model

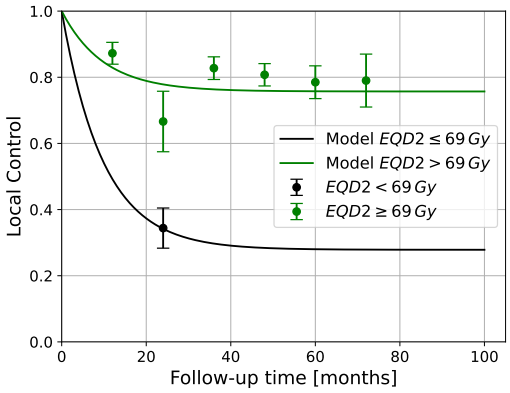

(c) TE model

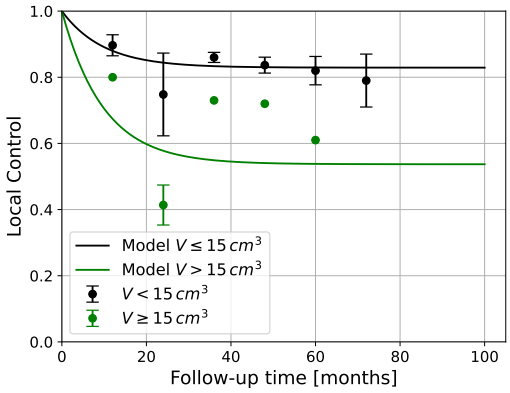

(d) TE model

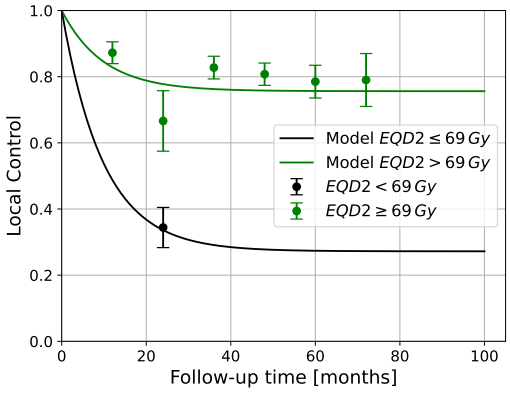

(e) TE model*

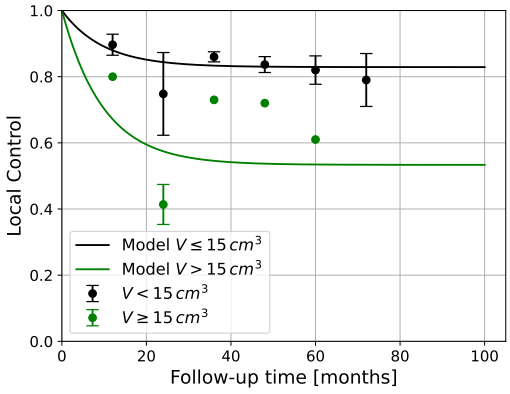

(f) TE model*

Figure 5 Local control as a function of follow-up time for pyriform sinus across all models categorized by total dose (left panel) and tumor volume (right panel). The TE model marked with a star (*) correspond to the variant, where the q value was estimated using the low-dose approximation. Error bars represent the standard error of the mean LC for each category at the specified follow-up time.

3.2 Breast

3.2.1 Volume Data

Table 10 Summary of LQ and TE model parameters for breast fitting the volume dataset. The table lists the estimated values for each parameter, along with their 95% confidence intervals (CI). Statistical significance levels are indicated based on the p_{wald} values. Parameters marked with a star (*) correspond to the TE model, where q was obtained by Equation (2.20) using the low-dose approximation. The CI of the calculated α/β ratio and q were derived using Gaussian error propagation.

Parameter [unit]	Value [95% CI]	p_{wald}
TCP_{pop}	$0.30\ [0.22, 0.39]$	< 0.01
λ [months^{-1}]	$0.04\ [0.03, 0.06]$	< 0.01
α [Gy^{-1}]	$0.12\ [0.12, 0.29]$	< 0.05
σ_α [Gy^{-1}]	$0.03\ [0.01, 0.04]$	< 0.01
β [Gy^{-2}]	$0.1\ [0.01, 0.099]$	< 0.01
α/β [Gy]	$1.19\ [0.27, 2.11]$	
p [Gy^{-1}]	$0.31\ [0.12, 0.32]$	< 0.01
σ_p [Gy^{-1}]	$0.03\ [0.01, 0.05$	$= 0.159$
q [Gy^{-1}]	$0.12\ [0.02, 0.6]$	$= 0.464$
p^* [Gy^{-1}]	$0.15\ [0.15, 0.20]$	< 0.01
σ_p^* [Gy^{-1}]	$0.04\ [0.01, 0.17]$	$= 0.178$
q^* [Gy^{-1}]	$0.52\ [0.38, 0.66]$	

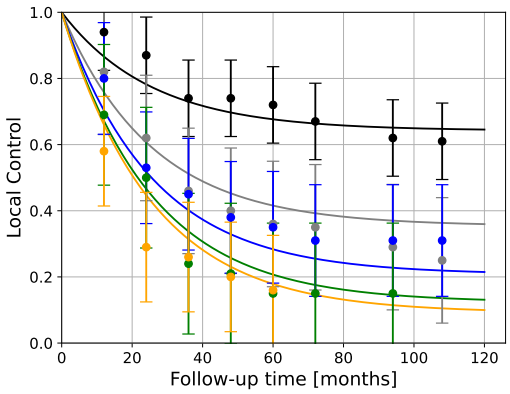

(a) LQ model

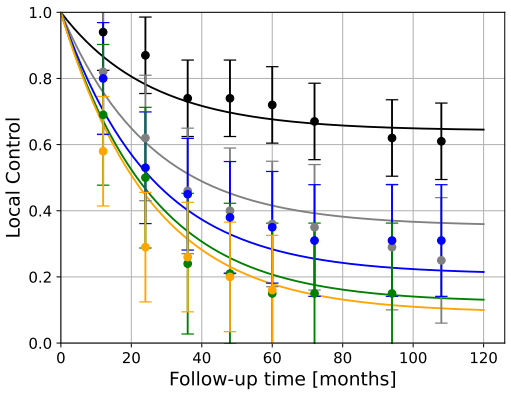

(b) TE model

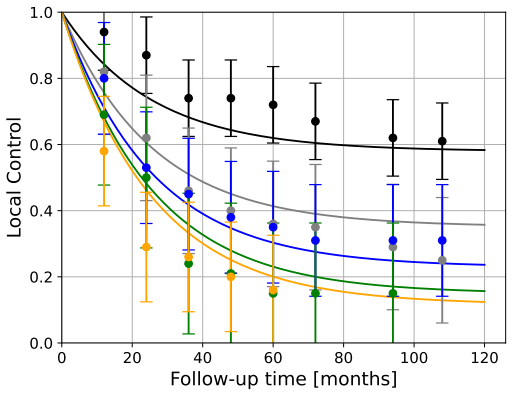

(c) TE model*

Figure 6 Local control as a function of follow-up time for different tumor size categories across all models. Tumor size categories are distinguished by color coding: $< 4\,\text{cm}$ (black), $4-6\,\text{cm}$ (grey), $6-8\,\text{cm}$ (blue), $8-10\,\text{cm}$ (green), and $\geq 10\,\text{cm}$ (orange). Error bars represent the standard error of the data point in the respective tumor size category. The TE model marked with a star (*) correspond to the variant, where the q value was estimated using the low-dose approximation.

3.2.2 Dose Data

Table 11 Summary of LQ and TE model parameters for breast fitting the dose dataset. The table lists the estimated values for each parameter, along with their 95% confidence intervals (CI). Statistical significance levels are indicated based on the p_{wald} values. Parameters marked with a star (*) correspond to the TE model, where q was obtained by Equation (2.20) using the low-dose approximation. The CI of the calculated α/β ratio and q were derived using Gaussian error propagation.

Parameter [unit]	Value [95% CI]	p_{wald}
TCP_{pop}	$0.39\ [0.25, 0.48]$	< 0.01
λ [months^{-1}]	$0.05\ [0.03, 0.09]$	< 0.01
α [Gy^{-1}]	$0.16\ [0.14, 0.38]$	< 0.05
σ_α [Gy^{-1}]	$0.15\ [0.07, 0.31]$	< 0.01
β [Gy^{-2}]	$0.07\ [0.0, 0.09]$	< 0.01
α/β [Gy]	$2.19\ [0.07, 4.3]$	
p [Gy^{-1}]	$0.27\ [0.17, 0.31]$	< 0.01
σ_p [Gy^{-1}]	$0.15\ [0.13, 0.17]$	< 0.01
q [Gy^{-1}]	$0.22\ [0.02, 0.48]$	$= 0.094$
p^* [Gy^{-1}]	$0.16\ [0.16, 0.21]$	< 0.01
σ_p^* [Gy^{-1}]	$0.15\ [0.11, 0.18]$	< 0.01
q^* [Gy^{-1}]	$0.48\ [0.28, 0.68]$	

The parameters obtained by fitting the TCP model to data from macroscopic tumor volumes treated with RT alone, are now used to determine the residual microscopic average tumor volume after surgery. Assuming the recurrence probabilities after surgery ($P_{\text{S}} = 0.2$) and after surgery combined with RT ($P_{\text{S-RT}} = 0.05$) [85], we can calculate the probability of recurrence after RT alone:

$$P_{\text{RT}} = \frac{P_{\text{S-RT}}}{P_{\text{S}}} = \frac{0.05}{0.2} = 0.25 \tag{3.1}$$

The tumor control probability for RT alone, which represents the recurrence-free probability, is:

$$\text{TCP}_{\text{RT}} = 1 - P_{RT} = 1 - 0.25 = 0.75. \tag{3.2}$$

By solving Equations (2.32) and (2.33) with respect to tumor volume and setting $\text{TCP} = 0.75$, we can estimate the remaining average tumor volume after surgery for a typical fractionation regimen of 30×2 Gy. The calculated average volume values, along with the number of remaining cells for each model, are presented in Table 12.

The corresponding mass values were calculated by assuming that tumor cells have a density equal to that of water (1 g/cm^3).

Table 12 Estimated average tumor volume $\bar{V}$, number of remaining cells N, and corresponding mass m after surgery, calculated for a typical fractionation regimen of 30×2 Gy using the LQ and TE model. The TE model marked with a star (*) correspond to the variant, where the q value was estimated using the low-dose approximation.

	$\bar{V}$ [cm^3]	N	m [g]
LQ model	0.087	874′227	0.087
TE model	0.087	872′458	0.087
TE model*	0.088	876′458	0.088

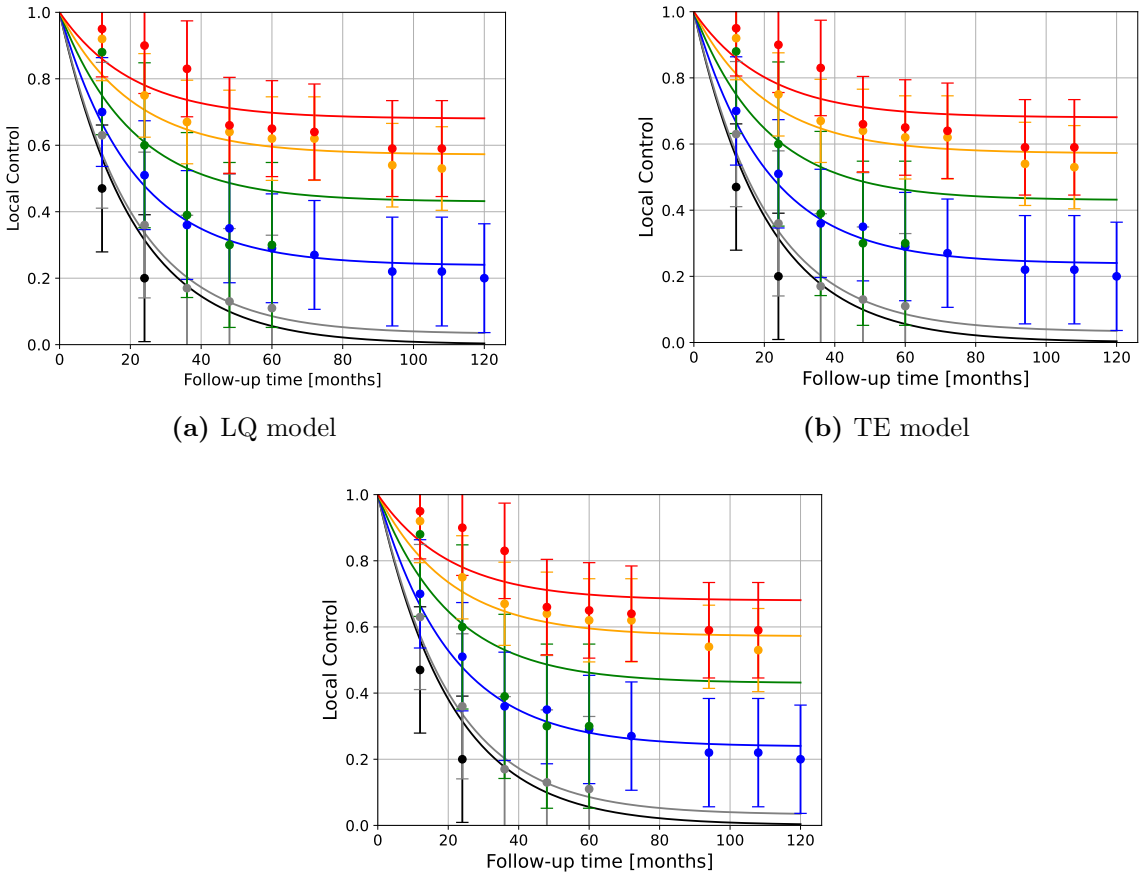

(a) LQ model

(b) TE model

(c) TE model*

Figure 7 Local control as a function of follow-up time for different dose categories across all models. Dose categories are distinguished by color coding: > 80 Gy (red), 70 – 80 Gy (orange), 60 – 70 Gy (green), 50 – 60 Gy (blue), 40 – 50 Gy (grey), and ≤ 40 Gy (black). Error bars represent the standard error of the data point in the respective dose category. The TE model marked with a star (*) correspond to the variant, where the q value was estimated using the low-dose approximation.

3.3 NSCLC

Table 13 Summary of LQ and TE model parameters for NSCLC. The table lists the estimated values for each parameter, along with their 95% confidence intervals (CI). Statistical significance levels are indicated based on the p_{wald} values. Parameters marked with a star (*) correspond to the TE model, where q was obtained by Equation (2.20) using the low-dose approximation. The CI of the calculated α/β ratio and q were derived using Gaussian error propagation.

Parameter [unit]	Value [95% CI]	p_{wald}
TCP_{pop}	$0.68\ [0.56, 0.74]$	< 0.01
λ [months^{-1}]	$0.08\ [0.03, 0.14]$	< 0.05
α [Gy^{-1}]	$0.32\ [0.25, 0.43]$	< 0.01
σ_α [Gy^{-1}]	$0.32\ [0.16, 0.39]$	< 0.01
β [Gy^{-2}]	$0.02\ [0.0, 0.02]$	< 0.01
α/β [Gy]	$21.8\ [12.55, 31.05]$	
p [Gy^{-1}]	$0.24\ [0.17, 0.43]$	< 0.01
σ_p [Gy^{-1}]	$0.24\ [0.13, 0.38]$	< 0.01
q [Gy^{-1}]	$0.39\ [0.17, 0.45]$	< 0.01
p^* [Gy^{-1}]	$0.28\ [0.24, 0.31]$	< 0.01
σ_p^* [Gy^{-1}]	$0.26\ [0.12, 0.3]$	< 0.01
q^* [Gy^{-1}]	$0.35\ [0.31, 0.39]$	

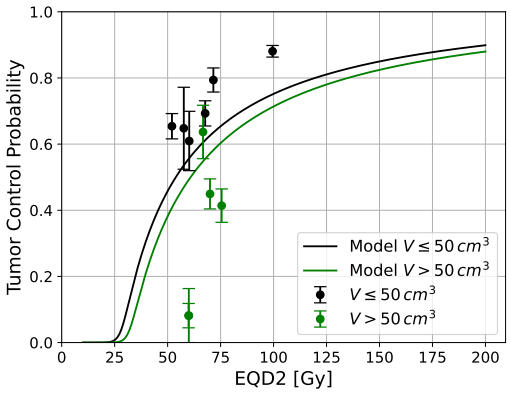

(a) LQ model

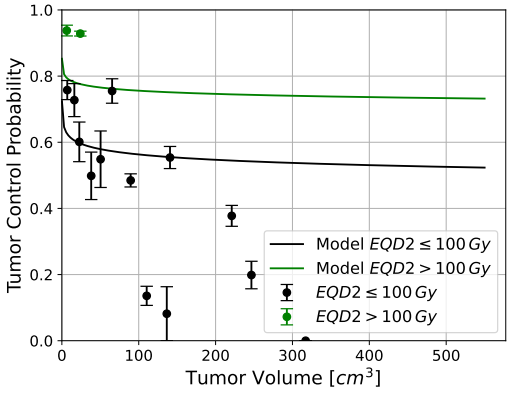

(b) LQ model

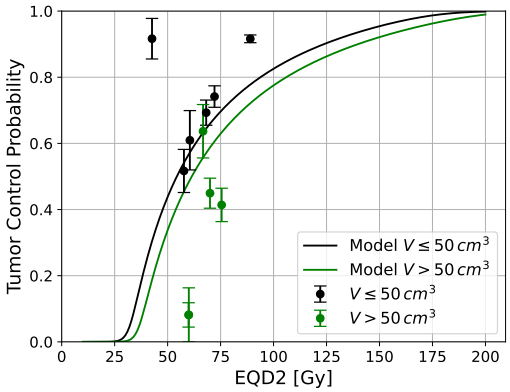

(c) TE model

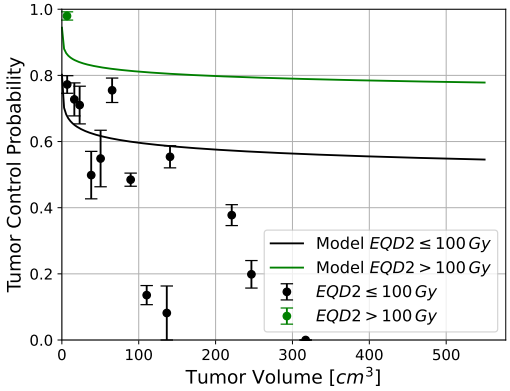

(d) TE model

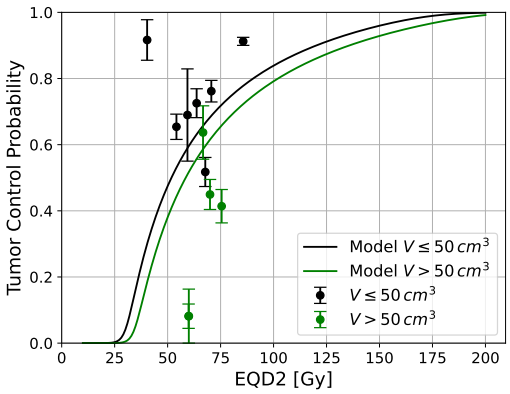

(e) TE model*

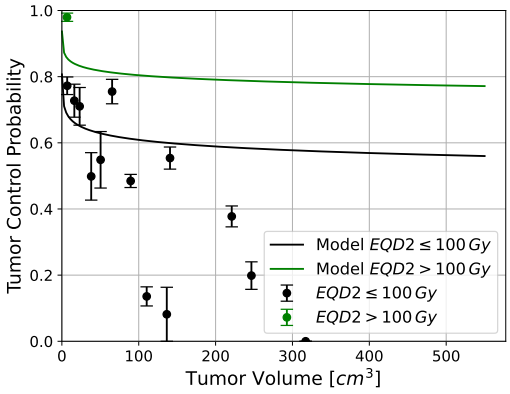

(f) TE model*

Figure 8 Tumor control probability as a function of dose and tumor volume for NSCLC across all models. The TE model marked with a star (*) correspond to the variant, where the q value was estimated using the low-dose approximation. The left panel shows tumor control probability as a function of dose, while the right panel shows tumor control probability as a function of tumor volume. The TCP model (solid line) is depicted, based on the average total dose and tumor volume in each category, and the found parameters from fit to the complete data set. Error bars represent the standard error of the mean TCP for each group at the respective dose/volume value.

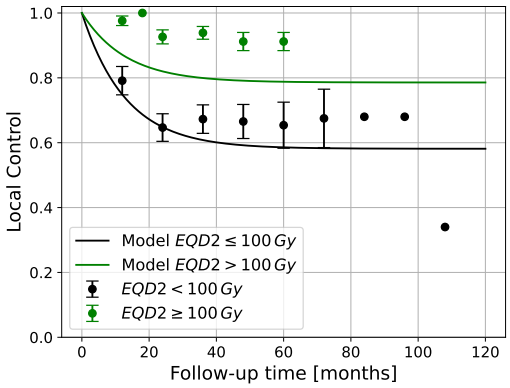

(a) LQ model

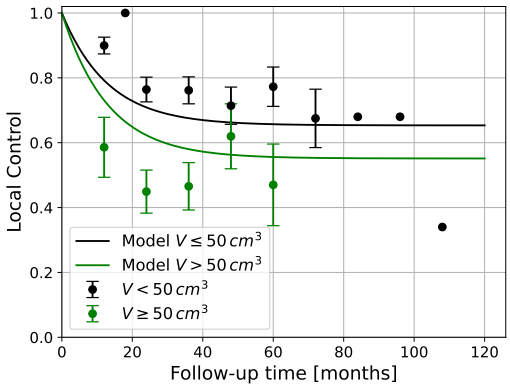

(b) LQ model

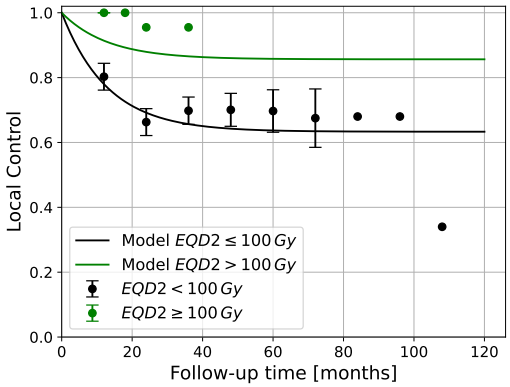

(c) TE model

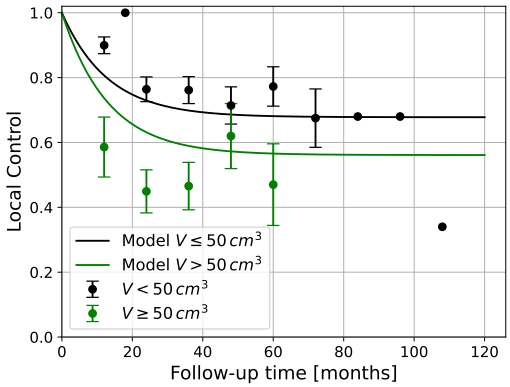

(d) TE model

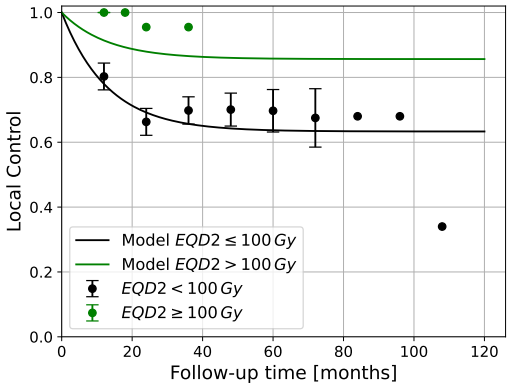

(e) TE model*

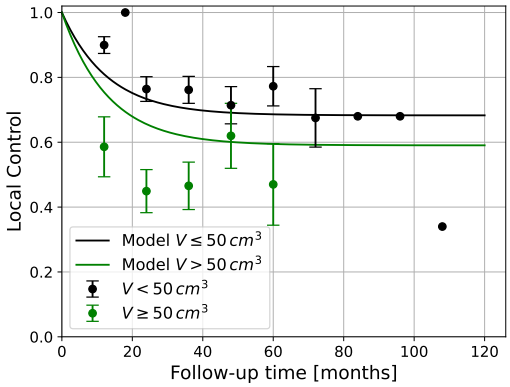

(f) TE model*

Figure 9 Local control as a function of follow-up time for NSCLC across all models categorized by total dose (left panel) and tumor volume (right panel). The TE model marked with a star (*) correspond to the variant, where the q value was estimated using the low-dose approximation. Error bars represent the standard error of the mean LC for each category at the specified follow-up time.

3.4 Brain Metastases

Table 14 Summary of LQ and TE model parameters for brain metastases. The table lists the estimated values for each parameter, along with their 95% confidence intervals (CI). Statistical significance levels are indicated based on the p_{wald} values. Parameters marked with a star (*) correspond to the TE model, where q was obtained by Equation (2.20) using the low-dose approximation. The CI of the calculated α/β ratio and q were derived using Gaussian error propagation.

Parameter [unit]	Value [95% CI]	p_{wald}
TCP_{pop}	$0.59\ [0.1, 0.78]$	< 0.05
$\lambda\ [\text{months}^{-1}]$	$0.05\ [0.01, 0.08]$	< 0.05
$\alpha\ [\text{Gy}^{-1}]$	$0.62\ [0.41, 0.98]$	< 0.01
$\sigma_\alpha\ [\text{Gy}^{-1}]$	$0.62\ [0.25, 0.93]$	< 0.01
$\beta\ [\text{Gy}^{-2}]$	$0.01\ [0.0, 0.02]$	< 0.01
$\alpha/\beta\ [\text{Gy}]$	$53.09\ [-14.41, 120.59]$	
$p\ [\text{Gy}^{-1}]$	$0.76\ [0.49, 0.88]$	< 0.01
$\sigma_p\ [\text{Gy}^{-1}]$	$0.76\ [0.44, 0.85]$	< 0.01
$q\ [\text{Gy}^{-1}]$	$0.23\ [0.05, 0.43]$	< 0.05
$p^*\ [\text{Gy}^{-1}]$	$0.43\ [0.37, 0.48]$	< 0.01
$\sigma_p^*\ [\text{Gy}^{-1}]$	$0.43\ [0.3, 0.46]$	< 0.01
$q^*\ [\text{Gy}^{-1}]$	$0.47\ [0.39, 0.55]$	

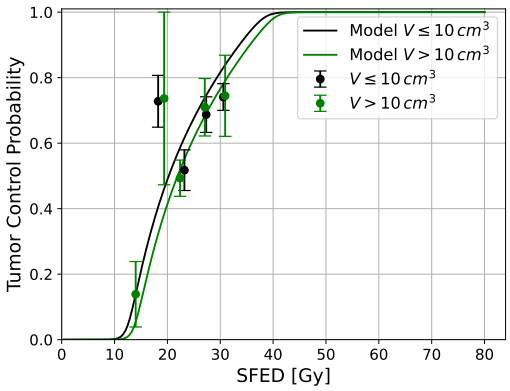

(a) LQ model

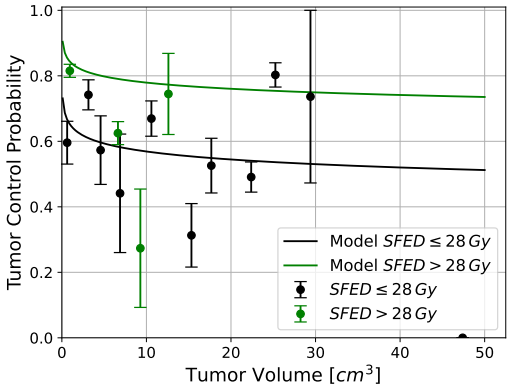

(b) LQ model

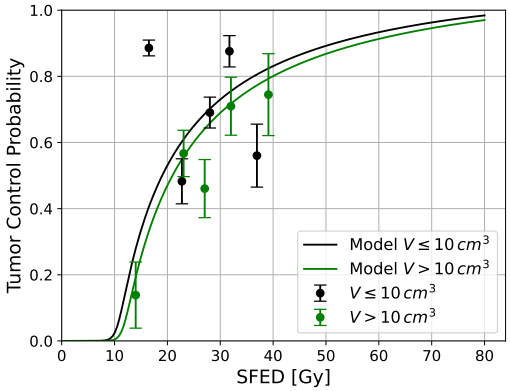

(c) TE model

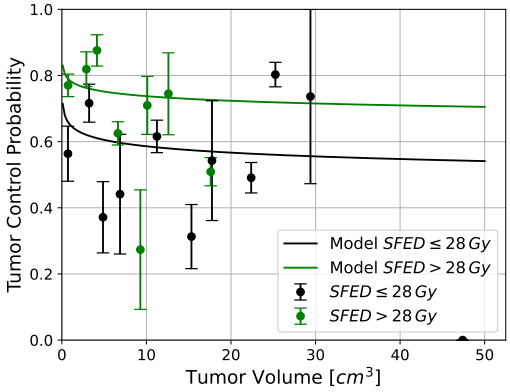

(d) TE model

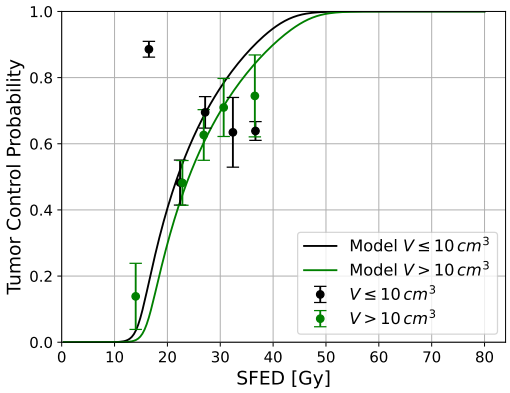

(e) TE model*

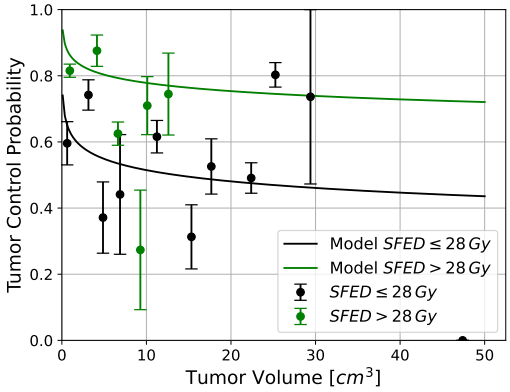

(f) TE model*

Figure 10 Tumor control probability as a function of dose and tumor volume for brain metastases across all models. The TE model marked with a star (*) correspond to the variant, where the q value was estimated using the low-dose approximation. The left panel shows tumor control probability as a function of dose, while the right panel shows tumor control probability as a function of tumor volume. The TCP model (solid line) is depicted based on the average total dose and tumor volume in each category, and the found parameters from fit to the complete data set. Error bars represent the standard error of the mean TCP for each group at the respective dose/volume value.

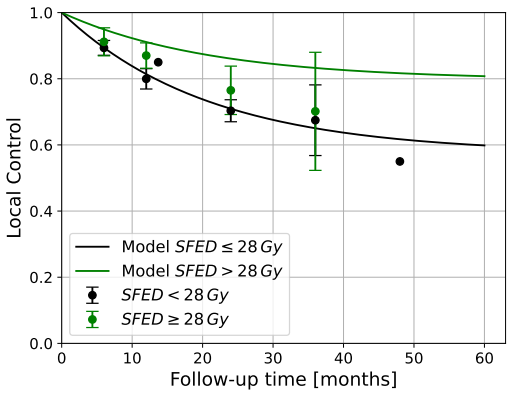

(a) LQ model

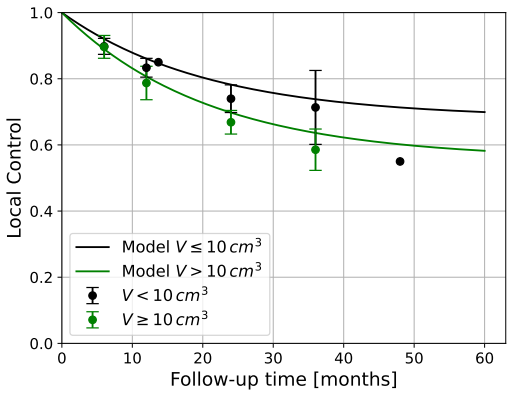

(b) LQ model

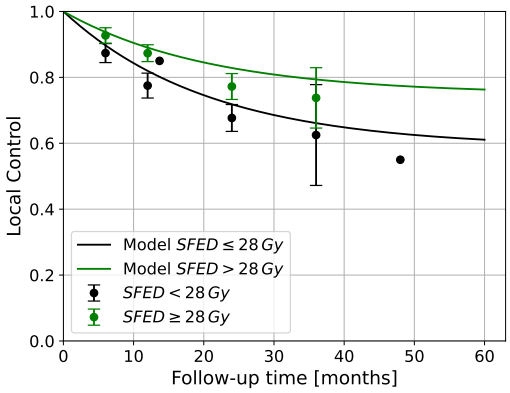

(c) TE model

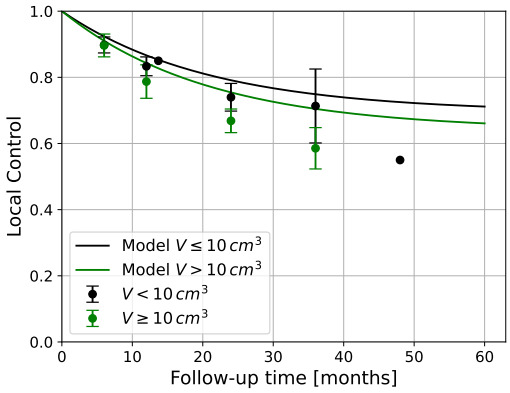

(d) TE model

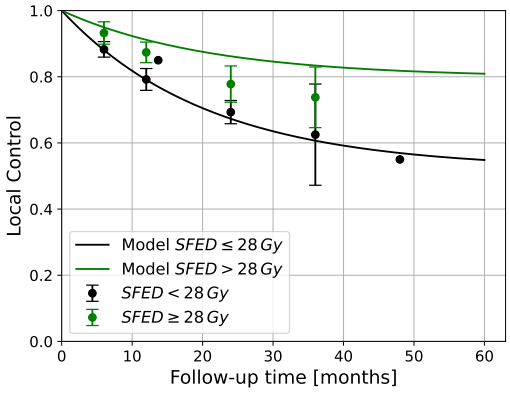

(e) TE model*

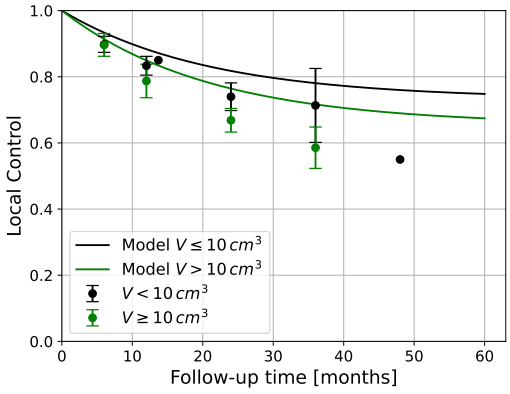

(f) TE model*

Figure 11 Local control as a function of follow-up time for brain metastases across all models categorized by total dose (left panel) and tumor volume (right panel). The TE model marked with a star (*) correspond to the variant, where the q value was estimated using the low-dose approximation. Error bars represent the standard error of the mean LC for each category at the specified follow-up time.

3.5 Model Performance Analysis

Table 15 presents the maximum log-likelihood values obtained for the fits of the LQ model, TE model, and the TE model* variant, where q was calculated using Equation (2.20) under the low-dose approximation. To facilitate a meaningful comparison across tumor sites with differing dataset sizes, the log-likelihood values were normalized by dividing the raw maximum log-likelihood values by the number of data points in each dataset. The normalization factors used are as follows: pyriform sinus (33), breast (dose: 37), breast (volume: 36), NSCLC (130), and brain metastases (99). In this context, a higher normalized log-likelihood value indicates a better model fit.

Table 15 Normalized maximum log-likelihood values for different models across all tumor sites. To allow comparison across datasets of varying sizes, the log-likelihood values are normalized by dividing the raw maximum log-likelihood by the number of data points in each dataset. The normalization factors are as follows: pyriform sinus (33), breast (dose: 37), breast (volume: 36), NSCLC (130), and brain metastases (99). Higher values indicate a better fit.

	LQ model	TE model	TE model*
Pyriform sinus	−3.4	−3.4	−3.4
Breast (dose)	−2.9	−2.9	−2.9
Breast (volume)	−3	−3	−3
NSCLC	−5.3	−5.2	−5.5
Brain metastases	−5.4	−6	−6.2

3.6 Radiation Necrosis

3.6.1 Single-Fraction Treatments

For the single-fraction treatment data the exponential model yielded a Vx_{50} of 39.31 $[12.3, 60.0]$ cm^3 and a slope γ_{50} of 0.85 $[0.33, 0.94]$. Both parameters were highly statistically significant, as confirmed by the Wald test ($p_{\text{wald}} < 0.01$). The normalized maximimum log-likelihood value for the exponential model was −7.29, obtained by dividing the raw maximum log-likelihood value by the number of data points in the single-fraction treatment dataset (= 15).

In contrast, the logarithmic form of the model indicated a higher volume, with Vx_{50} at 63.29 $[12.59, 70.0]$ cm^3, and a shallower slope of $\gamma_{50} = 0.26$ $[0.11, 0.57]$. While γ_{50} remained highly significant ($p_{\text{wald}} < 0.01$), the Vx_{50} parameter showed only moderate significance ($p_{\text{wald}} < 0.05$). The normalized maximum log-likelihood value for the logarithmic model was −6.2.

Figure 12 shows the relationship between V12 and the probability of symptomatic radiation necrosis for single-fraction treatments. The red curve illustrates the fit of the exponential model, while the blue curve represents the fit of its logarithmic form.

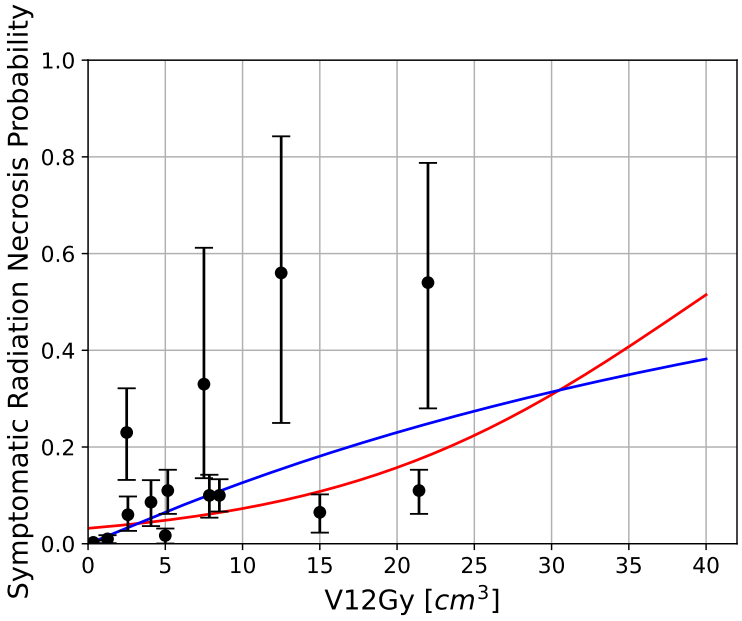

Figure 12 Probability of symptomatic radiation necrosis as a function of V12 for single-fraction treatments. The solid red and blue curves represent the fits for the exponential model and its logarithmic form, respectively. V12 refers to the brain volume receiving 12 Gy. Using the wald method, the error bars represent the weight of each data point by considering the number of patients. Larger samples yield narrower error bars, reflecting a higher weight.

3.6.2 Multi-Fraction Treatments

For multi-fraction treatments, comprising 16 data points, the brain volumes receiving x Gy (Vx) were converted to single-fraction 12 Gy volumes (V12). To calculate V12, the single-fraction equivalent dose was determined using either the LQ model or the TE model.

Using the LQ model, our exponential model estimated $\mathrm{Vx}_{50} = 62.46\ [43.72, 97.08]\ \mathrm{cm}^3$ and $\gamma_{50} = 1.05\ [0.91, 1.16]$, with a normalized maximum log-likelihood value of −2.66. The logarithmic form returned even a higher Vx_{50} of $185.04\ [172.34, 198.28]\ \mathrm{cm}^3$, but a shallower slope of $\gamma_{50} = 0.28\ [0.25, 0.29]$. The normalized maximum log-likelihood value was −2.87. Both models yielded highly statistically significant parameters ($p_{\mathrm{Wald}} < 0.01$).

When calculating V12 with the SFED equation derived by the TE model, the fitted parameter estimates were $\mathrm{Vx}_{50} = 82.54\ [59.65, 123.34]\ \mathrm{cm}^3$ and $\gamma_{50} = 1.05\ [0.92, 1.17]$ for the exponential form, with a normalized maximum log-likelihood value of −2.65. The logarithmic form estimated $\mathrm{Vx}_{50} = 153.57\ [132.14, 187.25]\ \mathrm{cm}^3$ and $\gamma_{50} = 0.33\ [0.29, 0.36]$, with a normalized maximum log-likelihood value of −3.44. Again, all parameter estimates were highly statistically significant ($p_{\mathrm{Wald}} < 0.01$).

The fits of the two models to the multi-fraction treatment data are shown in Figure 13. The left panel displays the results where the calculation of the SFED is based on the LQ model, while the right panel shows those based on the TE model.

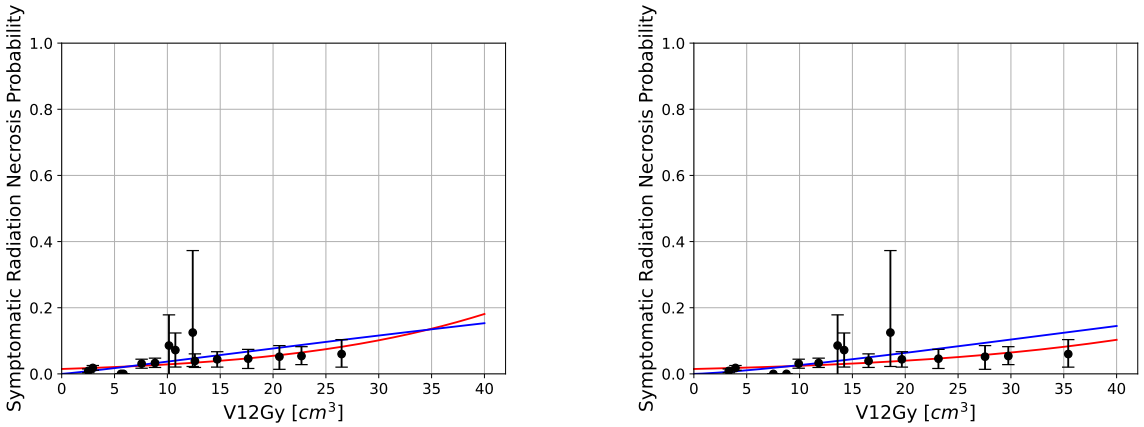

(a) (b)

Figure 13 Probability of symptomatic radiation necrosis as a function of V12 for multi-fraction treatments. In subplot (a), V12 is calculated using the single-fraction equivalent dose derived from the LQ model, while in subplot (b) the SFED is calculated using the TE model. The red curve represents the fit of the exponential model, and the blue curve shows the fit of the logarithmic form. The error bars represent the weight of each data point by considering the number of patients.

3.7 Complication-free Tumor Control

By combining the models for TCP and P_{SRN}, the complication-free TCP has been derived. As illustrated in Figure 14, the optimal fractionation scheme for maximizing tumor control while minimizing complications induced by radiation necrosis is tumor volume-dependent. The volumes where curves of different fractionation schedules intersect, indicate tumor volumes where one regimen becomes more favorable than another. Table 16 lists these intersection volumes, at which one particular fractionation schedule yields a higher complication-free TCP compared to another. For example, for tumor volumes below 24.97 cm^3, the 1×24 Gy schedule is preferable to the 3×7 Gy schedule. However, for tumor volumes exceeding 24.97 cm^3, the 3×7 Gy schedule becomes more favorable than 1×24 Gy.

Table 16 Volumes in cm^3 at intersection points of complication-free TCP curves in Figure 14 for different fractionation schemes. These intersection points indicate the tumor volumes at which one fractionation regimen achieves a higher complication-free TCP compared to another. TE* stands for the TE model variant where q was obtained by Equation (2.20) using the low-dose approximation.

	1×24 Gy $\cap$ 3×7 Gy	1×24 Gy $\cap$ 5×5 Gy	1×20 Gy $\cap$ 3×7 Gy	1×20 Gy $\cap$ 5×5 Gy
Exponential model (LQ)	24.97	19.13	16.82	1.33
Logarithmic model (LQ)	-	24.33	16.13	0.95
Exponential model (TE)	14.87	5.12	-	-
Logarithmic model (TE)	12.45	1.8	-	-
Exponential model (TE*)	25.65	16.95	13.86	-
Logarithmic model (TE*)	-	19.07	9.95	-

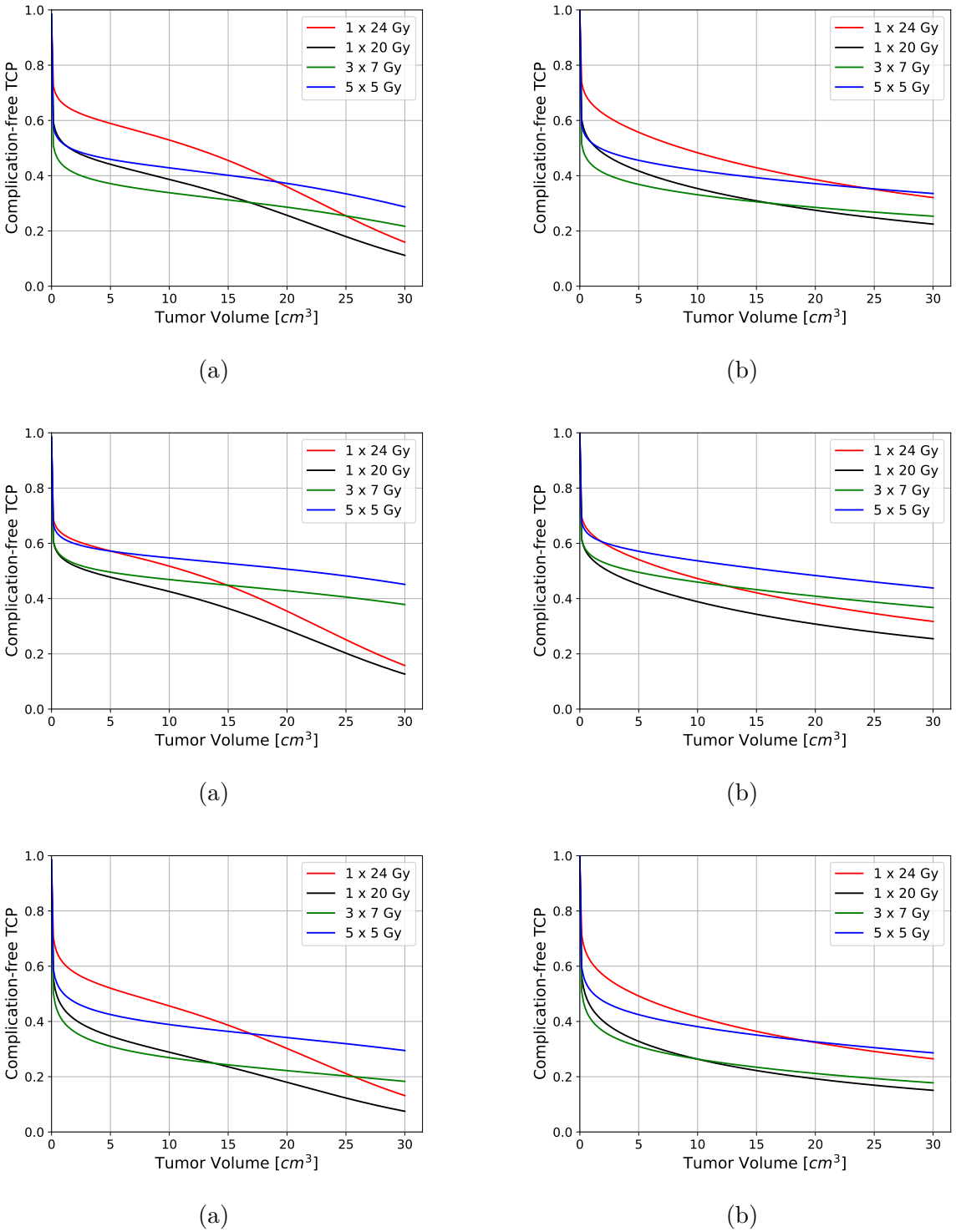

Figure 14 Complication-free TCP as a function of the tumor volume for various fractionation schedules. The left panel shows the complication-free TCP calculated using the exponential form of P_{SRN}, while the right panel displays the results using its logarithmic form. For the TCP model we used either the LQ model (a, b), the TE model (c, d) or the TE model with q obtained by Equation (2.20) using the low-dose approximation.

4 Discussion

In this work, a novel TCP population model was fitted to clinical data using two survival models: the LQ and the TE model. An empirical method proposed by Díaz et al. [1] was employed to evaluate the temporal evolution of local control in terms of TCP_{pop}. This method was applied to clinical data from four tumor sites: *pyriform sinus*, *breast*, *non-small cell lung cancer*, and *brain metastases*. For brain metastases, symptomatic radiation necrosis was also modeled, employing two simple logistic models to estimate its probability. A combination of the TCP_{pop} and SRN models, yields the complication-free tumor control probability, offering a method to select a volume specific optimal fractionation schedule for patients with brain metastases.

4.1 Tumor-Specific Findings

From the analysis of the fitted curves, we find a clear trend: higher doses and smaller tumor volumes are associated with increased tumor control (see Figure 4, 8 and 10). Introducing a variability in cell radiosensitivity results in an asymmetrical dose-response curve for NSCLC and brain metastases. Tumors in the dataset with radiosensitivity values α higher than the central fitted α value contribute to a steeper dose-response, reflecting a sharp increase in TCP at lower doses. Conversely, tumors with lower α values show a more gradual response, resulting in a slower overall rise in TCP as the dose increases. This highlights the significant impact of interpatient heterogeneity on treatment outcomes.
The results obtained from fitting the TE model using q derived from the low-dose approximation should be interpreted with caution. This approximation is valid only within a limited dose range, approximately up to 3 Gy [5]. Therefore, applying the resulting fitting parameters to high-dose treatments may lead to inaccuracies.

4.1.1 Pyriform Sinus

For pyriform sinus cancer, an $\frac{\alpha}{\beta}$ ratio of 1.64 $[0.09, 3.19]$ Gy was obtained, which is notably lower than the values reported in the literature. For example, Taylor et al. [86] estimated $\frac{\alpha}{\beta} = 7.8\ [3, \infty]$ Gy, although their study included other tumor sites within the larynx and hypopharynx. Similarly, Chappell et al. [87] reported a higher $\frac{\alpha}{\beta}$ ratio of 9.3 Gy using logistic regression to model local control.
The analysis confirms that TCP is highly dependent on tumor volume, with larger tumors showing a significant reduction in tumor control. As shown in Figure 5, local

control approaches TCP after a relatively short follow-up period of approximately 20 months. During this period, LC decreases by about 20% for an EQD2 above 69 Gy, while for an EQD2 below 69 Gy, the decrease is approximately 60%, as illustrated in the left panel of Figure 5. In the right panel of the same figure, the LC reduction is around 20% for tumor volumes smaller than 15 cm^3, compared to a decrease of approximately 45% for volumes larger than 15 cm^3.

4.1.2 Breast

The derived $\frac{\alpha}{\beta}$ ratio of 2.19 Gy for breast tumors aligns with the general trend in the literature that breast cancer exhibits a relatively low $\frac{\alpha}{\beta}$, indicating similar fractionation sensitivity as normal tissues. Qi et al. [88] estimated an $\frac{\alpha}{\beta}$ ratio of 3.89 Gy, but with a high uncertainty of 6.25 Gy. Similarly, Murray et al. [89] reported an $\frac{\alpha}{\beta}$ ratio of 3.7 $[0.3, 7.1]$ Gy from the FAST-Forward trial, closely matching the 3.5 $[1.2, 5.7]$ Gy found in the START pilot trials [90]. Our result of 2.19 Gy is slightly lower but within the broad confidence intervals of these studies.
The model parameters, obtained by fitting the TCP model to LC data for macroscopic tumors treated with radiotherapy alone (without surgery), can be applied to modern neoadjuvant radiotherapy. In this context, where surgery is followed by RT, the model allows for the determination of the residual microscopic tumor volume after surgery. This residual microscopic tumor volume can then be used to predict TCP for several commonly used fractionation schedules. Figure 15 presents these predictions, derived from three different modeling approaches: the LQ model (triangles), the TE model (stars) and the TE model where q was obtained by Equation (2.20) using the low-dose approximation (squares). The LQ model predicts higher TCP values compared to the other models. With the exception of the 5×5 Gy schedule, all fractionation schemes show similar TCP predictions, suggesting they are similarly effective in achieving tumor control. However, the 5×5 Gy schedule yields significantly lower TCP values, indicating that this regimen may be suboptimal for clinical use. Murray et al. [89] demonstrated that delivering 26 Gy in five fractions is equivalent to 40 Gy in 15 fractions and 27 Gy in five fractions in terms of local control. While the LQ model accurately captures this trend, the TE model shows significant differences between the three fractionation schedules. Regarding normal tissue effects such as breast distortion or shrinkage, the 5×5.2 Gy was found to be non-inferior to the standard 15×2.67 Gy [89]. It is important to note that these side effects, which were not accounted for in our models, can also influence tumor control outcomes. Today, it is also common to treat breast tumors with RT in combination with chemotherapy or hormone therapy, neither of which is considered in this work.

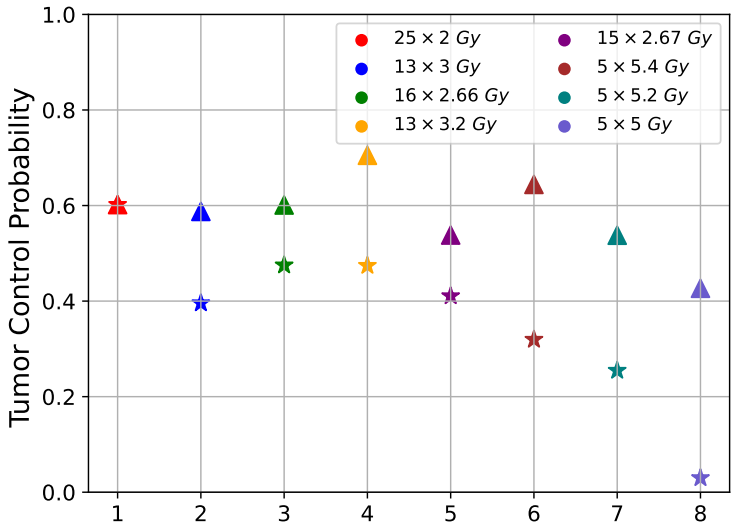

Figure 15 Tumor control probability predictions for breast cancer under different typical adjuvant fractionation schedules used in the clinic. The TCP predictions were generated using the LQ model (triangles), the TE model (stars), and the modified TE model where q was obtained by Equation (2.20) using the low-dose approximation (squares). The LQ model generally predicts higher TCP values compared to the the TE model. All schedules, except 5×5 Gy, show comparable TCP values, indicating similar effectiveness in tumor control. The 5×5 Gy schedule shows significantly lower TCP, making it less suitable for clinical use.

4.1.3 NSCLC

The analysis of the NSCLC dataset yielded a fitted $\frac{\alpha}{\beta}$ ratio of 21.8 Gy. This value is consistent with studies that account for tumor regrowth dynamics, in particular with those by Liu et al. [91] and Maciejewski et al. [92], which suggest that rapidly repopulating tumors tend to exhibit higher $\frac{\alpha}{\beta}$ ratios.

The volume dependence, illustrated in the right panel of Figure 8, shows significance primarily for very small tumors. For larger volumes, the variations in TCP become much smaller. The left panel of Figure 9 illustrates that after a follow-up time of 40 months, the local control decreases by approximately 35% for an EQD2 below 100 Gy, whereas for an EQD2 above 100 Gy, the decrease is only around 15%. In the right panel of the same figure, the LC reduction is about 40% for tumor volumes exceeding 50 cm^3, compared to a 30% reduction for volumes smaller than 50 cm^3.

Figure 16 displays TCP predictions for NSCLC RT across various fractionation schedules and tumor volumes. The results show the expected trend: TCP increases as tumor volume decreases, regardless of the fractionation schedule or model. Among the evaluated regimes, the 3×18 Gy schedule yields the highest TCP values regardless of the survival model. The TE models (both standard and modified) predict nearly identical TCP values across all fractionation regimens. The LQ model predicts higher TCP values for the 1×32 Gy and 3×18 Gy schedules compared to the TE models. For

the other three fractionation schedules, the LQ model predicts lower TCP values. As tumor volume increases, these differences between the LQ and TE model predictions become less significant. It is important to note that NSCLC tumors are known for their rapid repopulation during radiotherapy [87], a critical factor that can significantly impact treatment outcomes. Incorporating a repopulation correction into the TCP models could account for this dynamic, potentially altering parameter estimates and, consequently, TCP predictions.

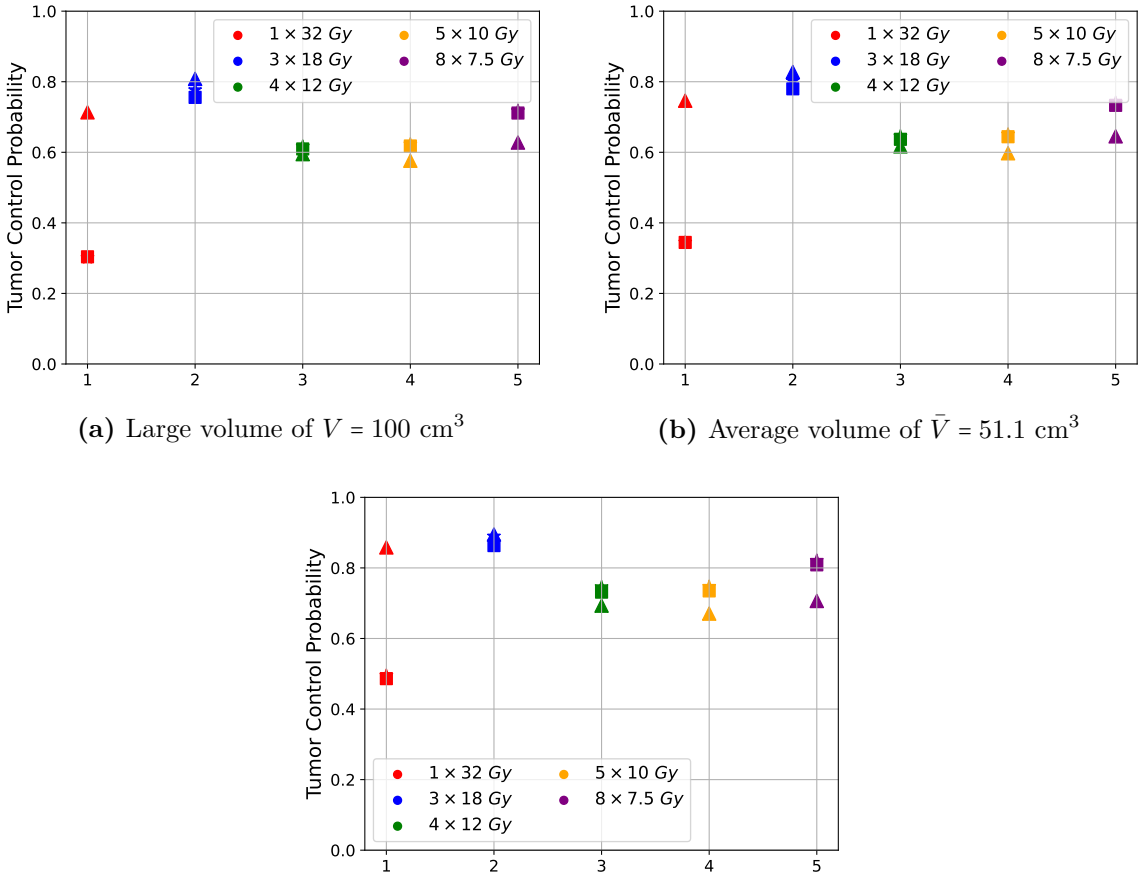

(a) Large volume of $V = 100$ cm^3

(b) Average volume of $\bar{V} = 51.1$ cm^3

(c) Small volume of $V = 5$ cm^3

Figure 16 Tumor control probability predictions for NSCLC under different fractionation schedules and tumor volumes. Predictions were generated using three models: the LQ model (triangles), the TE model (stars), and the modified TE model (squares) where q was obtained by Equation (2.20) using the low-dose approximation. Each subplot represents a different tumor volume: (a) large ($V = 100$ cm^3), (b) average ($\bar{V} = 51.1$ cm^3), and (c) small ($V = 5$ cm^3).

4.1.4 Brain Metastases and Symptomatic Radiation Necrosis

After fitting the models to the brain metastases data, an exceptionally high $\frac{\alpha}{\beta}$ ratio of 53.09 Gy was observed. However, this result aligns with the findings of Redmond et al. [48], where maximum-likelihood parameter searches for brain metastases also

yielded $\frac{\alpha}{\beta} \geq 20$. The fitted p and σ_p value should be interpreted with caution for brain metastases. Since p represents the probability of a lethal event, the sum of p and its variation σ_p must remain within the range $[0, 1]$. To ensure more realistic fitting parameters, this constraint should be explicitly incorporated into the maximum likelihood estimation process. Similar to NSCLC, the volume dependence for tumor control in brain metastases is primarily evident for smaller tumor volumes.

Figure 17 displays TCP and 1-year LC predictions for different fractionation schedules, commonly used in clinical practice. These results demonstrate a significant benefit for fractionated treatments over single-fraction regimens. Notably, the LQ model consistently predicts lower TCP and LC values than the TE model. Interestingly, the newly proposed 15×4 Gy regimen [93] appears to outperform the standard therapies used to date. However, when accounting for potential side effects such as symptomatic radiation necrosis, the optimal fractionation schedule for a patient may change according to volume. As shown in Figure 14, the curves for the four selected fractionation schedules intersect, indicating that the preferred fractionation schedule depends on the tumor volume. The intersection volumes, listed in Table 16, highlight the tumor volume at which one regimen becomes more favorable over another. According to both, the LQ model and the TE model variant incorporating the LQ model's $\frac{\alpha}{\beta}$ ratio, tumor volumes of ≤ 20 cm^3 are best treated with a single fraction of 1×24 Gy. For tumor volumes exceeding this threshold, the 5×5 Gy regimen is recommended. Larger tumors (≥ 25 cm^3) are best treated with a 3×7 Gy schedule, particularly under the exponential model for symptomatic radiation necrosis (left panel). Conversely, the standard TE model favors fractionated treatments even at smaller volumes (≤ 5 cm^3). Among all regimens, the 1×20 Gy consistently performs worst in the TE model. Appendix Figure A1 shows TCP as a function of tumor volume for the four different fractionation schedules across all models. This figure provides a comparison to Figure 14, highlighting the impact of SRN on the complication-free TCP. In this thesis, the probabilities of tumor control and symptomatic radiation necrosis are assumed to be independent. However this assumption may not fully reflect reality. While some patients may exhibit independent responses in their tumors and normal tissues, a subset of patients could experience dependent responses. To address this limitations, the formulation of complication-free TCP proposed by Lind et al. [84] should be considered. This approach incorporates both independent and dependent responses using a weighting factor δ, which represents the proportion of patients with independent responses. By introducing δ, the model allows for a linear combination of independent and dependent probabilities, providing a more realistic estimation of complication-free TCP.

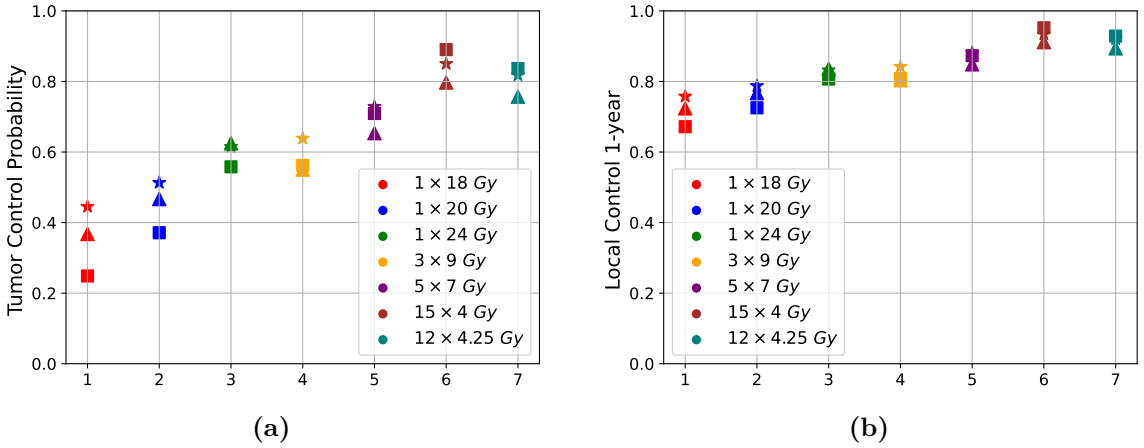

Figure 17 Tumor control probability (a) and 1-year local control (b) predictions for brain metastases under different fractionation schedules for the mean cohort volume of 5.07 cm^3. The predictions were generated using the LQ model (triangles), the TE model (stars), and the modified TE model where q was obtained by Equation (2.20) using the low-dose approximation (squares).

The fitted curves of the SRN models closely match those presented in Milano et al. [73], confirming their reliability. From a graphical perspective, the logarithmic model demonstrates closer alignment with the curves reported in Milano et al. [73] for both single- and multi-fraction treatment data. For single-fraction treatment data, this alignment is further supported by the normalized maximum log-likelihood value, which favor the logarithmic model. In contrast, for multi-fraction treatment data, the exponential model provides a better fit, as indicated by higher normalized maximum log-likelihood values.

Single-fraction treatments appear to exhibit a higher probability of inducing SRN compared to mutli-fraction treatments. However, the simplified models used in this work account for fractionation only in a limited manner, through the calculation of V12. To address this limitation, a more comprehensive NTCP model, such as those proposed by Lyman-Kutcher or Zaider [77], should be considered. Incorporating an NTCP model that explicitly accounts for the effects of fractionation, would allow for the simultaneous fitting of both single-fraction and multi-fraction treatment studies.

4.2 Model Comparison and Outlook

For tumor sites, where only conventionally fractionated treatments were considered (pyriform sinus and breast), a direct comparison between the LQ and TE model is not possible, as the TE model converges to the LQ model at low doses. As a result, both models show identical performance in fitting the data, which is confirmed by their identical maximum log-likelihood values in Table 15. In the case of NSCLC,

where both conventional and hypofractionated datasets were analyzed, the TE model provides a slightly better fit, as evidenced by its larger log-likelihood value compared to the LQ model. However, for tumor sites treated only with hypofractionation, such as brain metastases, the TE model performs worse than the LQ model, as reflected in the lower log-likelihood value.

While the LQ model has a long history of clinical use and has demonstrated effectiveness over decades, the TE model is a relatively new approach, having been introduced only a decade ago. Replacing a well-established model like the LQ, which has consistently guided clinical practice, presents a significant challenge. However, the potential of the TE model, particularly for hypofractionated treatments, warrants further investigation. Extensive testing on diverse datasets and clinical studies will be necessary to validate its accuracy and reliability. With continued research and validation, the TE model may one day be considered a valuable tool in the planning of hypofractionated treatment regimens.

4.3 Biological Considerations and Model Limitations

Although the TCP model presented in this work provides crucial insights, it does not capture the full complexity of radiobiological processes. Fractionation effects are governed by key mechanisms such as repair, redistribution, reoxygenation, and repopulation [3]. These phenomena, collectively known as the "4 Rs" of radiobiology, significantly influence treatment outcomes. Incorporating these factors into the model would require additional parameters, increasing model complexity and the risk of over-fitting. However, such integration could improve the biological fidelity of TCP predictions.

Furthermore, the sensitivity of cells to radiation varies throughout the phases of the cell cycle. Cells in the G2 and M phases tend to be more radiosensitive, whereas those in the S phase are relatively radioresistant [6]. By integrating cell cycle dynamics into the model, it would be possible to better account for variations in cell damage based on the timing of radiation exposure.

Including these biological factors would enhance the predictive power of the TCP model, offering deeper insights into the interplay between fractionation and cellular response to radiation. Nevertheless, the novel TCP model presented in this work captures the essential dynamics by accounting for variability in cell sensitivity. This approach simplifies the model by reducing secondary dependencies on factors mentioned above. As a result, it effectively averages out the influence of these variables, making the model more manageable.

A Appendix

A.1 Initial Parameter Ranges for Maximum Likelihood Optimization

In order to optimize the log-likelihood and determine the best-fitting parameters for the models, we first need to define initial parameter ranges that are biologically plausible. These ranges serve as the starting point for the grid search algorithm, which iteratively narrows down the search space based on the results from each iteration. The initial ranges of the parameters α, σ_α, and β for the LQ model are provided in Table A1 for the different tumor sites. Similarly, the initial ranges of the parameters corresponding to the TE model are given in Table A2. For λ and $\mathrm{TCP_{pop}}$ the ranges were set to [0.001, 0.1] s^{-1} and [0.1, 1.0], respectively. The initial parameter ranges for the SRN model fits are displayed in Table A3.

Table A1 Initial parameter ranges for the parameter fitting of the LQ model. The parameters include α, σ_α and β with their respective units. For breast, two different datasets are fitted seperately: one categorized by dose groups and the other by volume groups.

	α [$\mathrm{Gy^{-1}}$]	σ_α [$\mathrm{Gy^{-1}}$]	β [$\mathrm{Gy^{-2}}$]
Pyriform sinus	[0.1, 0.5]	[0.01, 0.4]	[0.01, 0.1]
Breast (dose)	[0.1, 0.5]	[0.01, 0.4]	[0.01, 0.1]
Breast (volume)	[0.1, 0.5]	[0.01, 0.4]	[0.01, 0.1]
NSCLC	[0.1, 0.5]	[0.01, 0.4]	[0.001, 0.1]
Brain metastases	[0.1, 0.8]	[0.01, 1.0]	[0.001, 0.1]

Table A2 Initial parameter ranges for the parameter fitting of the TE model. The parameters include p, σ_p and q with their respective units. For breast, two different datasets are fitted seperately: one categorized by dose groups and the other by volume groups.

	p [$\mathrm{Gy^{-1}}$]	σ_p [$\mathrm{Gy^{-1}}$]	q [$\mathrm{Gy^{-1}}$]
Pyriform sinus	[0.1, 0.5]	[0.01, 0.4]	[0.001, 0.1]
Breast (dose)	[0.1, 1.0]	[0.01, 0.4]	[0.001, 0.1]
Breast (volume)	[0.1, 1.0]	[0.01, 0.4]	[0.001, 1.0]
NSCLC	[0.1, 1.0]	[0.01, 0.4]	[0.001, 1.0]
Brain metastases	[0.1, 0.9]	[0.01, 1.0]	[0.001, 0.5]

Table A3 Initial parameter ranges for the parameter fitting of the symptomatic radiation necrosis models. The parameters include γ_{50} and Vx_{50} with their respective units.

	γ_{50}	Vx_{50} [cm^3]
Exponential model (SF)	[0.1, 1.0]	[1, 60]
Logarithmic mode (SF)	[0.1, 1.0]	[1, 70]
Exponential model (MF, LQ)	[0.1, 1.5]	[1, 150]
Exponential model (MF, TE)	[0.1, 1.5]	[1, 150]
Logarithmic model (MF, LQ)	[0.1, 1.0]	[1, 210]
Logarithmic model (MF, TE)	[0.1, 2.5]	[1, 170]

A.2 Summary of Estimated Model Parameters

In this section, we present a summary of the estimated parameters obtained through model fitting for different tumor types and radiation treatments. The parameters derived from the LQ model and the TE model variant where q was obtained by Equation (2.20) using the low-dose approximation are provided in Table A4, while those from the SRN models are shown in Table A5.

Table A4 Summary of estimated parameters for the LQ model and the TE model across different tumor sites. Here, q was obtained by Equation (2.20) using the low-dose approximation.

	λ [s^{-1}]	α [Gy^{-1}]	σ_α [Gy^{-1}]	β [Gy^{-2}]	α/β [Gy]	p [Gy^{-1}]	σ_p [Gy^{-1}]	q [Gy^{-1}]
Pyriform sinus	0.10	0.15	0.09	0.089	1.64	0.16	0.09	0.52
Breast (dose)	0.05	0.16	0.07	0.001	2.19	0.16	0.16	0.48
Breast (volume)	0.04	0.12	0.03	0.1	1.19	0.15	0.05	0.52
NSCLC	0.08	0.32	0.32	0.02	21.8	0.28	0.26	0.35
Brain metastases	0.05	0.62	0.62	0.01	53.09	0.43	0.43	0.47

Table A5 Summary of estimated parameters (γ_{50} and Vx_{50}) for different SRN models (exponential and logarithmic) across two treatment modes. The SF (single-fraction) and MF (multi-fraction) represent the two different treatment modes. For MF treatments, V12 has to be calculated using either the SFED equation derived from the LQ model or the TE model.

	γ_{50}	Vx_{50} [cm^3]
Exponential model (SF)	0.85	39.31
Logarithmic model (SF)	0.26	63.29
Exponential model (MF, LQ)	1.05	62.46
Exponential model (MF, TE)	1.05	82.54
Logarithmic model (MF, LQ)	0.28	185.04
Logarithmic model (MF, TE)	0.33	153.57

A.3 TCP in Brain Metastases as a Function of Tumor volume

Figure A1 illustrates TCP as a function of tumor volume for brain metastases, based on the different survival models. This plot provides a direct comparison to Figure 14, enabling the evaluation of the separate contributions of TCP and SRN to the overall complication-free TCP.

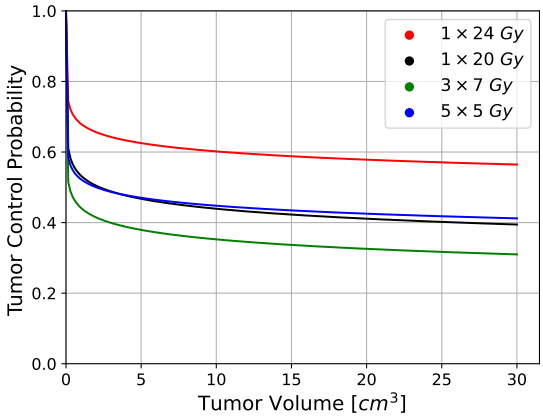

(a) LQ model

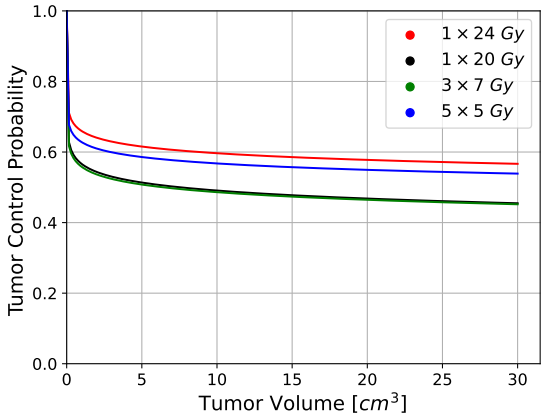

(b) TE model

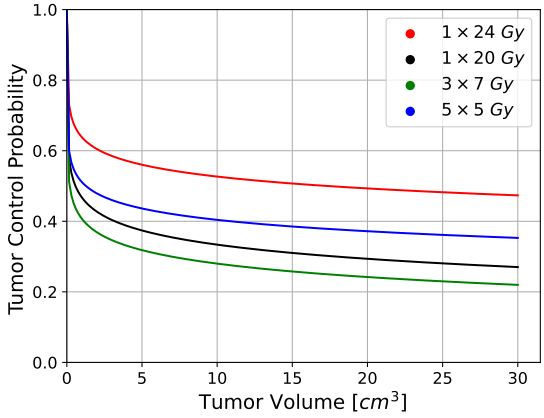

(c) TE model*

Figure A1 Tumor control probability as a function of tumor volume for four selected fractionation schedules across three models: (a) LQ model, (b) TE model, and (c) TE model* with q obtained by Equation (2.20) using the low-dose approximation.

A.4 Gaussian Error Propagation

The confidence intervals for the calculated $\frac{\alpha}{\beta}$ ratio and the parameter q were derived using Gaussian error propagation. The uncertainty in the estimate of the parameter $\frac{\alpha}{\beta}$, is:

$$\mathrm{SE}(\alpha/\beta) = \sqrt{\left(\frac{\partial(\alpha/\beta)}{\partial\alpha}\,\mathrm{SE}(\alpha)\right)^2 + \left(\frac{\partial(\alpha/\beta)}{\partial\beta}\,\mathrm{SE}(\beta)\right)^2}. \tag{A.1}$$

For q, whose function is defined in Equation (2.19), the standard error is:

$$\mathrm{SE}(q) = \sqrt{\left(\frac{\partial q}{\partial p}\,\mathrm{SE}(p)\right)^2 + \left(\frac{\partial q}{\partial(\alpha/\beta)}\,\mathrm{SE}(\alpha/\beta)\right)^2}. \tag{A.2}$$

The standard errors (SE) of the individual parameters are derived from their 95% confidence intervals ($\mathrm{CI}_{\mathrm{upper}}, \mathrm{CI}_{\mathrm{lower}}$) using the formula:

$$\mathrm{SE} = \frac{\mathrm{CI}_{\mathrm{upper}} - \mathrm{CI}_{\mathrm{lower}}}{2 \times 1.96}. \tag{A.3}$$

Once the standard errors are calculated, the 95% confidence intervals for the derived parameters $\frac{\alpha}{\beta}$ and q are obtained as follows:

$$\mathrm{CI}_{\mathrm{upper}} = f + 1.96 \times \mathrm{SE}(f), \tag{A.4}$$

$$\mathrm{CI}_{\mathrm{lower}} = f - 1.96 \times \mathrm{SE}(f), \tag{A.5}$$

where f represents either $\frac{\alpha}{\beta}$ or q.

Bibliography

[1]K. Díaz, U. Schneider, J. Besserer, and S. Unterkirhers, "Realistic closed-form tcp model including dose and tumor volume dependence", Physics in Medicine Biology, Submitted for publication (2024).

[2]S. Radonic, J. Besserer, V. Meier, C. R. Bley, and U. Schneider, "A novel analytical population tumor control probability model includes cell density and volume variations: application to canine brain tumor", International Journal of Radiation Oncology*Biology*Physics **110**, 1530–1537 (2021).

[3]D. J. Brenner, "The linear-quadratic model is an appropriate methodology for determining isoeffective doses at large doses per fraction", Seminars in Radiation Oncology **18**, 234–239 (2008).

[4]T. Sheu, J. Molkentine, M. K. Transtrum, T. A. Buchholz, H. R. Withers, H. D. Thames, and K. A. Mason, "Use of the LQ model with large fraction sizes results in underestimation of isoeffect doses", Radiotherapy and Oncology **109**, 21–25 (2013).

[5]J. Besserer and U. Schneider, "A track-event theory of cell survival", Zeitschrift für Medizinische Physik **25**, 168–175 (2015).

[6]L. Jones, P. Hoban, and P. Metcalfe, "The use of the linear quadratic model in radiotherapy: a review", Australas. Phys. Eng. Sci. Med. **24**, 132–146 (2001).

[7]M. Ebert, "Radiation oncology physics: a handbook for teachers and students", Physics in Medicine Biology **51**, 1047 (2006).

[8]T. Munro and C. Gilbert, "The relation between tumour lethal doses and the radiosensitivity of tumour cells.", Br. J. Radiol. **34**, 246–251.

[9]S. Webb and A. E. Nahum, "A model for calculating tumour control probability in radiotherapy including the effects of inhomogeneous distributions of dose and clonogenic cell density", Phys. Med. Biol. **38**, 653–666 (1993).

[10]U. Schneider and J. Besserer, "Tumour volume distribution can yield information on tumour growth and tumour control", Zeitschrift für Medizinische Physik **32**, 143–148 (2022).

[11]P. Okunieff, D. Morgan, A. Niemierko, and H. D. Suit, "Radiation dose-response of human tumors", International Journal of Radiation Oncology*Biology*Physics **32**, 1227–1237 (1995).

[12]A. Nagai, Y. Shibamoto, M. Yoshida, K. Wakamatsu, and Y. Kikuchi, "Treatment of single or multiple brain metastases by hypofractionated stereotactic radiotherapy using helical tomotherapy", IJMS **15**, Publisher: MDPI AG, 6910–6924 (2014).

[13]S. B. Edge and American Joint Committee on Cancer, eds., *AJCC cancer staging manual*, 7th ed, OCLC: ocn316431417 (Springer, New York, 2010), 648 pp.

[14]Automeris, *Wpd: web page designer*, Accessed: 2024-09-29, 2024.

[15]R. Arriagada, H. Mouriesse, D. Sarrazin, R. Clark, and G. Deboer, "Radiotherapy alone in breast cancer. i. analysis of tumor parameters, tumor dose and local control: the experience of the gustave-roussy institute and the princess margaret hospital", International Journal of Radiation Oncology*Biology*Physics **11**, 1751–1757 (1985).

[16]F. Deng, *Pyriform sinus | radiology reference article | radiopaedia.org*, Radiopaedia, `https://radiopaedia.org/articles/pyriform-sinus?lang=us`.

[17]L. Döbrössy, "Epidemiology of head and neck cancer: magnitude of the problem", Cancer Metastasis Rev **24**, 9–17 (2005).

[18]P. Blanchard, Y. Tao, O. Veresezan, A. Lusinchi, A.-M. Le Ridant, F. Janot, N. Daly-Schveitzer, and J. Bourhis, "Definitive radiotherapy for squamous cell carcinoma of the pyriform sinus", Radiotherapy and Oncology **105**, 232–237 (2012).

[19]A. Nakajima, K. Nishiyama, M. Morimoto, S. Nakamura, O. Suzuki, Y. Kawaguchi, K. Miyagi, T. Fujii, and K. Yoshino, "Definitive radiotherapy for t1–2 hypopharyngeal cancer: a single-institution experience", International Journal of Radiation Oncology*Biology*Physics **82**, e129–e135 (2012).

[20]A. Rabbani, R. J. Amdur, A. A. Mancuso, J. W. Werning, J. Kirwan, C. G. Morris, and W. M. Mendenhall, "Definitive radiotherapy for t1-t2 squamous cell carcinoma of pyriform sinus", International Journal of Radiation Oncology*Biology*Physics **72**, 351–355 (2008).

[21]F. A. Pameijer, A. A. Mancuso, W. M. Mendenhall, J. T. Parsons, S. K. Mukherji, R. Hermans, and P. S. Kubilis, "Evaluation of pretreatment computed tomography as a predictor of local control in t1/t2 pyriform sinus carcinoma treated with definitive radiotherapy", Head Neck **20**, 159–168 (1998).

[22]P. Bataini, J. Brugere, J. Bernier, C. Jaulerry, C. Picot, and N. Ghossein, "Results of radical radiotherapeutic treatment of carcinoma of the pyriform sinus: experience of the institut curie", International Journal of Radiation Oncology*Biology*Physics **8**, 1277–1286 (1982).

[23]*Types of breast cancer | about breast cancer*, `https://www.cancer.org/cancer/types/breast-cancer/about/types-of-breast-cancer.html`.

[24]M. L. Czajka and C. Pfeifer, "Breast cancer surgery", in *StatPearls* (StatPearls Publishing, Treasure Island (FL), 2024).

[25]P. Lee, B. W. Loo, T. Biswas, G. X. Ding, I. M. El Naqa, A. Jackson, F.-M. Kong, T. LaCouture, M. Miften, T. Solberg, W. A. Tome, A. Tai, E. Yorke, and X. A. Li, "Local control after stereotactic body radiation therapy for stage i non-small cell lung cancer", International Journal of Radiation Oncology*Biology*Physics **110**, 160–171 (2021).

[26]J. D. Bradley, S. Wahab, M. A. Lockett, C. A. Perez, and J. A. Purdy, "Elective nodal failures are uncommon in medically inoperable patients with stage i non–small-cell lung carcinoma treated with limited radiotherapy fields", International Journal of Radiation Oncology*Biology*Physics **56**, 342–347 (2003).

[27]J. D. Bradley, N. Ieumwananonthachai, J. A. Purdy, T. H. Wasserman, M. A. Lockett, M. V. Graham, and C. A. Perez, "Gross tumor volume, critical prognostic factor in patients treated with three-dimensional conformal radiation therapy for non-small-cell lung carcinoma", International Journal of Radiation Oncology*Biology*Physics **52**, 49–57 (2002).

[28]H. M. Sandler, W. J. Curran, and A. T. Turrisi, "The influence of tumor size and pretreatment staging on outcome following radiation therapy alone for stage i non-small cell lung cancer", International Journal of Radiation Oncology*Biology*Physics **19**, 9–13 (1990).

[29]J. Willner and M. Flentje, "DOSE, VOLUME, AND TUMOR CONTROL PREDICTIONS IN PRIMARY RADIOTHERAPY OF NON–SMALL-CELL LUNG CANCER", **52** (2002).

[30]J. A. Bogart, T. E. Alpert, M. C. Kilpatric, B. L. Keshler, S. S. Pohar, H. Shah, E. Dexter, and J. N. Aronowitz, "Dose-intensive thoracic radiation therapy for patients at high risk with early-stage non–small-cell lung cancer", Clinical Lung Cancer **6**, 350–354 (2005).

[31]K. Hayakawa, N. Mitsuhashi, Y. Saito, Y. Nakayama, M. Furuta, H. Sakurai, M. Kawashima, T. Ohno, S. Nasu, and H. Niibe, "Limited field irradiation for medically inoperable patients with peripheral stage i non-small cell lung cancer", Lung Cancer (1999).

[32]P. C. Cheung, L. T. Yeung, V. Basrur, Y. C. Ung, J. Balogh, and C. E. Danjoux, "Accelerated hypofractionation for early-stage non-small-cell lung cancer", International Journal of Radiation Oncology*Biology*Physics **54**, 1014–1023 (2002).

[33]J. A. Langendijk, N. K. Aaronson, J. M. De Jong, G. P. Ten Velde, M. J. Muller, B. J. Slotman, and E. F. Wouters, "Quality of life after curative radiotherapy in stage i non-small-cell lung cancer", International Journal of Radiation Oncology*Biology*Physics **53**, 847–853 (2002).

[34]F. J. Lagerwaard, S. Senan, J. P. Van Meerbeeck, and W. J. Graveland, "Has 3-d conformal radiotherapy (3d CRT) improved the local tumour control for stage i non-small cell lung cancer?", Radiotherapy and Oncology **63**, 151–157 (2002).

[35]K. E. Rosenzweig, N. Dladla, R. Schindelheim, S. E. Sim, L. E. Braban, E. S. Venkatraman, and S. A. Leibel, "Three-dimensional conformal radiation therapy (3d-CRT) for early-stage non–small-cell lung cancer", Clinical Lung Cancer **3**, 141–144 (2001).

[36]Y. Shirata, K. Jingu, M. Koto, M. Kubozono, K. Takeda, T. Sugawara, N. Kadoya, and H. Matsushita, "Prognostic factors for local control of stage i non-small cell lung cancer in stereotactic radiotherapy: a retrospective analysis", Radiat Oncol **7**, Publisher: Springer Science and Business Media LLC, 10.1186/1748-717x-7-182 (2012).

[37]D. R. Oncobgy, "Volume and dose placaters for survival of non-small cell lung cancer patients", Radiotherapy and Oncology (1997).

[38]P. Fritz, H.-J. Kraus, T. Blaschke, W. Mühlnickel, K. Strauch, W. Engel-Riedel, A. Chemaissani, and E. Stoelben, "Stereotactic, high single-dose irradiation of stage i non-small cell lung cancer (NSCLC) using four-dimensional CT scans for treatment planning", Lung Cancer **60**, Publisher: Elsevier BV, 193–199 (2008).

[39]P. Baumann, J. Nyman, M. Hoyer, B. Wennberg, G. Gagliardi, I. Lax, N. Drugge, L. Ekberg, S. Friesland, K.-A. Johansson, J.-Å. Lund, E. Morhed, K. Nilsson, N. Levin, M. Paludan, C. Sederholm, A. Traberg, L. Wittgren, and R. Lewensohn, "Outcome in a prospective phase II trial of medically inoperable stage i non–small-cell lung cancer patients treated with stereotactic body radiotherapy", JCO **27**, Publisher: American Society of Clinical Oncology (ASCO), 3290–3296 (2009).

[40]K. L. Stephans, T. Djemil, C. A. Reddy, S. M. Gajdos, M. Kolar, D. Mason, S. Murthy, T. W. Rice, P. Mazzone, M. Machuzak, T. Mekhail, and G. M. Videtic, "A comparison of two stereotactic body radiation fractionation schedules for medically inoperable stage i non-small cell lung cancer: the cleveland clinic experience", Journal of Thoracic Oncology **4**, Publisher: Elsevier BV, 976–982 (2009).

[41]T. D. Crabtree, C. E. Denlinger, B. F. Meyers, I. El Naqa, J. Zoole, A. S. Krupnick, D. Kreisel, G. A. Patterson, and J. D. Bradley, "Stereotactic body radiation therapy versus surgical resection for stage i non–small cell lung cancer", The Journal of Thoracic and Cardiovascular Surgery **140**, Publisher: Elsevier BV, 377–386 (2010).

[42]R. Timmerman, R. Paulus, J. Galvin, J. Michalski, W. Straube, J. Bradley, A. Fakiris, A. Bezjak, G. Videtic, D. Johnstone, J. Fowler, E. Gore, and H. Choy, "Stereotactic body radiation therapy for inoperable early stage lung cancer",

[43]G. M. Videtic, K. Stephans, C. Reddy, S. Gajdos, M. Kolar, E. Clouser, and T. Djemil, "Intensity-modulated radiotherapy–based stereotactic body radiotherapy for medically inoperable early-stage lung cancer: excellent local control", International Journal of Radiation Oncology*Biology*Physics **77**, Publisher: Elsevier BV, 344–349 (2010).

[44]Y. Shibamoto, C. Hashizume, F. Baba, S. Ayakawa, Y. Manabe, A. Nagai, A. Miyakawa, T. Murai, H. Iwata, Y. Mori, M. Mimura, and S. Ishikura, "Stereotactic body radiotherapy using a radiobiology-based regimen for stage i nonsmall cell lung cancer: a multicenter study", Cancer **118**, Publisher: Wiley, 2078–2084 (2012).

[45]A. Takeda, N. Sanuki, T. Eriguchi, T. Kaneko, S. Morita, H. Handa, Y. Aoki, Y. Oku, and E. Kunieda, "Stereotactic ablative body radiation therapy for octogenarians with non-small cell lung cancer", International Journal of Radiation Oncology*Biology*Physics **86**, Publisher: Elsevier BV, 257–263 (2013).

[46]M. Hamaji, F. Chen, Y. Matsuo, A. Kawaguchi, S. Morita, N. Ueki, M. Sonobe, Y. Nagata, M. Hiraoka, and H. Date, "Video-assisted thoracoscopic lobectomy versus stereotactic radiotherapy for stage i lung cancer", The Annals of Thoracic Surgery **99**, Publisher: Elsevier BV, 1122–1129 (2015).

[47]J.-C. M. Rwigema, A. M. Chen, P.-C. Wang, J. M. Lee, E. Garon, and P. Lee, "Incidental mediastinal dose does not explain low mediastinal node recurrence rates in patients with early-stage NSCLC treated with stereotactic body radiotherapy", Clinical Lung Cancer **15**, Publisher: Elsevier BV, 287–293 (2014).

[48]K. J. Redmond, C. Gui, S. Benedict, M. T. Milano, J. Grimm, J. A. Vargo, S. G. Soltys, E. Yorke, A. Jackson, I. El Naqa, L. B. Marks, J. Xue, D. E. Heron, and L. R. Kleinberg, "Tumor control probability of radiosurgery and fractionated stereotactic radiosurgery for brain metastases", International Journal of Radiation Oncology*Biology*Physics **110**, 53–67 (2021).

[49]A. M. Baschnagel, K. D. Meyer, P. Y. Chen, D. J. Krauss, R. E. Olson, D. R. Pieper, A. H. Maitz, H. Ye, and I. S. Grills, "Tumor volume as a predictor of survival and local control in patients with brain metastases treated with gamma knife surgery: clinical article", JNS **119**, Publisher: Journal of Neurosurgery Publishing Group (JNSPG), 1139–1144 (2013).

[50]P. H. Ko, H. J. Kim, J. S. Lee, and W. C. Kim, "Tumor volume and sphericity as predictors of local control after stereotactic radiosurgery for limited number (1-4) brain metastases from nonsmall cell lung cancer", Asia-Pac J Clncl Oncology **16**, Publisher: Wiley, 165–171 (2020).

[51]Y. Higuchi, T. Serizawa, O. Nagano, S. Matsuda, J. Ono, M. Sato, Y. Iwadate, and N. Saeki, "Three-staged stereotactic radiotherapy without whole brain irradiation for large metastatic brain tumors", International Journal of Radiation Oncology*Biology*Physics **74**, Publisher: Elsevier BV, 1543–1548 (2009).

[52]J. Lutterbach, D. Cyron, K. Henne, and C. B. Ostertag, "Radiosurgery followed by planned observation in patients with one to three brain metastases", Neurosurgery **52**, Publisher: Ovid Technologies (Wolters Kluwer Health), 1066–1074 (2003).

[53]J.-i. Saitoh, Y. Saito, T. Kazumoto, S. Kudo, A. Ichikawa, N. Hayase, K. Kazumoto, H. Sakai, and K. Shibuya, "Therapeutic effect of linac-based stereotactic radiotherapy with a micro-multileaf collimator for the treatment of patients with brain metastases from lung cancer", Japanese Journal of Clinical Oncology **40**, Publisher: Oxford University Press (OUP), 119–124 (2010).

[54]H. Aoyama, H. Shirato, R. Onimaru, K. Kagei, J. Ikeda, N. Ishii, Y. Sawamura, and K. Miyasaka, "Hypofractionated stereotactic radiotherapy alone without whole-brain irradiation for patients with solitary and oligo brain metastasis using noninvasive fixation of the skull", International Journal of Radiation Oncology*Biology*Physics **56**, Publisher: Elsevier BV, 793–800 (2003).

[55]P. Lindvall, P. Bergström, P.-O. Löfroth, R. Henriksson, and A. T. Bergenheim, "Hypofractionated conformal stereotactic radiotherapy alone or in combination with whole-brain radiotherapy in patients with cerebral metastases", International Journal of Radiation Oncology*Biology*Physics **61**, Publisher: Elsevier BV, 1460–1466 (2005).

[56]K. Tokuuye, Y. Akine, M. Sumi, Y. Kagami, S. Murayama, H. Nakayama, H. Ikeda, M. Tanaka, S. Shibui, and K. Nomura, "Fractionated stereotactic radiotherapy of small intracranial malignancies", International Journal of Radiation Oncology*Biology*Physics **42**, Publisher: Elsevier BV, 989–994 (1998).

[57]A. Jani, T. Rozenblat, A. M. Yaeh, T. Nanda, S. Saad, Y. H. Qureshi, W. Feng, M. B. Sisti, J. N. Bruce, G. M. McKhann, J. Lesser, A. B. Lassman, S. R. Isaacson, and T. J. C. Wang, "The energy index does not affect local control of brain metastases treated by gamma knife stereotactic radiosurgery", Neurosurgery **77**, Publisher: Ovid Technologies (Wolters Kluwer Health), 119–125 (2015).

[58]G. Minniti, V. Esposito, E. Clarke, C. Scaringi, G. Lanzetta, M. Salvati, A. Raco, A. Bozzao, and R. Maurizi Enrici, "Multidose stereotactic radiosurgery (9 gy × 3) of the postoperative resection cavity for treatment of large brain metastases", International Journal of Radiation Oncology*Biology*Physics **86**, Publisher: Elsevier BV, 623–629 (2013).

[59]M. K. Shehata, B. Young, B. Reid, R. A. Patchell, W. St. Clair, J. Sims, M. Sanders, A. Meigooni, M. Mohiuddin, and W. F. Regine, "Stereotatic radiosurgery of 468 brain metastases 2 cm: implications for SRS dose and whole brain radiation therapy", International Journal of Radiation Oncology*Biology*Physics **59**, Publisher: Elsevier BV, 87–93 (2004).

[60]L. Feuvret, S. Vinchon, V. Martin, I. Lamproglou, A. Halley, V. Calugaru, M. Chea, C. Valéry, J.-M. Simon, and J.-J. Mazeron, "Stereotactic radiotherapy for large solitary brain metastases", Cancer/Radiothérapie **18**, Publisher: Elsevier BV, 97–106 (2014).

[61]T. Murai, H. Ogino, Y. Manabe, M. Iwabuchi, T. Okumura, Y. Matsushita, Y. Tsuji, H. Suzuki, and Y. Shibamoto, "Fractionated stereotactic radiotherapy using CyberKnife for the treatment of large brain metastases: a dose escalation study", Clinical Oncology **26**, Publisher: Elsevier BV, 151–158 (2014).

[62]F. Zairi, Y. Ouammou, E. Le Rhun, R. Aboukais, S. Blond, M. Vermandel, V. Deken, P. Devos, and N. Reyns, "Relevance of gamma knife radiosurgery alone for the treatment of non-small cell lung cancer brain metastases", Clinical Neurology and Neurosurgery **125**, Publisher: Elsevier BV, 87–93 (2014).

[63]R. E. Elliott, S. C. Rush, A. Morsi, N. Mehta, J. Spriet, A. Narayana, B. Donahue, E. C. Parker, and J. G. Golfinos, "Local control of newly diagnosed and distally recurrent, low-volume brain metastases with fixed-dose (20 gy) gamma knife radiosurgery", Neurosurgery **68**, Publisher: Ovid Technologies (Wolters Kluwer Health), 921–931 (2011).

[64]T. Matsuo, S. Shibata, A. Yasunaga, M. Iwanaga, K. Mori, T. Shimizu, N. Hayashi, M. Ochi, and K. Hayashi, "Dose optimization and indication of linac radiosurgery for brain metastases", International Journal of Radiation Oncology*Biology*Physics **45**, Publisher: Elsevier BV, 931–939 (1999).

[65]B. J. Blonigen, R. D. Steinmetz, L. Levin, M. A. Lamba, R. E. Warnick, and J. C. Breneman, "Irradiated volume as a predictor of brain radionecrosis after linear accelerator stereotactic radiosurgery", International Journal of Radiation Oncology*Biology*Physics **77**, Publisher: Elsevier BV, 996–1001 (2010).

[66]H. K. Inoue, H. Sato, K.-i. Seto, K. Torikai, Y. Suzuki, J.-i. Saitoh, S.-e. Noda, and T. Nakano, "Five-fraction CyberKnife radiotherapy for large brain metastases in critical areas: impact on the surrounding brain volumes circumscribed with a single dose equivalent of 14 gy (v14) to avoid radiation necrosis", Journal of Radiation Research **55**, Publisher: Oxford University Press (OUP), 334–342 (2014).

[67]G. Minniti, C. Scaringi, S. Paolini, E. Clarke, F. Cicone, V. Esposito, A. Romano, M. Osti, and R. M. Enrici, "Repeated stereotactic radiosurgery for patients with progressive brain metastases", J Neurooncol **126**, Publisher: Springer Science and Business Media LLC, 91–97 (2016).

[68]G. Minniti, R. M. D'Angelillo, C. Scaringi, L. E. Trodella, E. Clarke, P. Matteucci, M. F. Osti, S. Ramella, R. M. Enrici, and L. Trodella, "Fractionated stereotactic radiosurgery for patients with brain metastases", J Neurooncol **117**, Publisher: Springer Science and Business Media LLC, 295–301 (2014).

[69]G. Minniti, E. Clarke, G. Lanzetta, M. F. Osti, G. Trasimeni, A. Bozzao, A. Romano, and R. M. Enrici, "Stereotactic radiosurgery for brain metastases: analysis of outcome and risk of brain radionecrosis", Radiat Oncol **6**, 48 (2011).

[70]Y. Jiao, F. Cao, and H. Liu, "Radiation-induced cell death and its mechanisms", Health Physics, `10.1097/HP.0000000000001601` (2022).

[71]A. Fabiano, D. Prasad, and J. Qiu, "Adverse radiation effect in the brain during cancer radiotherapy", J Radiat Cancer Res **8**, 135 (2017).

[72]V. Cuccurullo, G. D. Di Stasio, G. L. Cascini, G. Gatta, and C. Bianco, "The molecular effects of ionizing radiations on brain cells: radiation necrosis vs. tumor recurrence", Diagnostics **9**, 127 (2019).

[73]M. T. Milano, J. Grimm, A. Niemierko, S. G. Soltys, V. Moiseenko, K. J. Redmond, E. Yorke, A. Sahgal, J. Xue, A. Mahadevan, A. Muacevic, L. B. Marks, and L. R. Kleinberg, "Single- and multifraction stereotactic radiosurgery dose/volume tolerances of the brain", International Journal of Radiation Oncology*Biology*Physics **110**, 68–86 (2021).

[74]B. Zhao, N. Wen, I. J. Chetty, Y. Huang, S. L. Brown, K. C. Snyder, F. Siddiqui, B. Movsas, and M. S. Siddiqui, "A prediction model of radiation-induced necrosis for intracranial radiosurgery based on target volume", Medical Physics **44**, 4360–4367 (2017).

[75]T. Korytko, T. Radivoyevitch, V. Colussi, B. W. Wessels, K. Pillai, R. J. Maciunas, and D. B. Einstein, "12 gy gamma knife radiosurgical volume is a predictor for radiation necrosis in non-AVM intracranial tumors", International Journal of Radiation Oncology*Biology*Physics **64**, 419–424 (2006).

[76]K. Ohtakara, S. Hayashi, N. Nakayama, N. Ohe, H. Yano, T. Iwama, and H. Hoshi, "Significance of target location relative to the depth from the brain surface and high-dose irradiated volume in the development of brain radionecrosis after micromultileaf collimator-based stereotactic radiosurgery for brain metastases", J Neurooncol **108**, 201–209 (2012).

[77]M. Zaider and H. Amols, "Practical considerations in using calculated healthy-tissue complication probabilities for treatment-plan optimization", International Journal of Radiation Oncology*Biology*Physics **44**, 439–447 (1999).

[78]B. Emami, J. Lyman, A. Brown, L. Cola, M. Goitein, J. Munzenrider, B. Shank, L. Solin, and M. Wesson, "Tolerance of normal tissue to therapeutic irradiation", International Journal of Radiation Oncology*Biology*Physics **21**, 109–122 (1991).

[79]E. J. Lehrer, A. A. Khosla, A. Ozair, J. Gurewitz, K. Bernstein, D. Kondziolka, A. Niranjan, Z. Wei, L. D. Lunsford, D. Mathieu, C. Trudel, C. P. Deibert, T. D. Malouff, H. Ruiz-Garcia, J. L. Peterson, S. Patel, P. Bonney, L. Hwang, C. Yu, G. Zada, P. Picozzi, A. Franzini, L. Attuati, R. N. Prasad, R. R. Raval, J. D. Palmer, C.-c. Lee, H.-c. Yang, K. R. Fakhoury, C. G. Rusthoven, D. R. Dickstein, J. P. Sheehan, D. M. Trifiletti, and M. S. Ahluwalia, "Immune checkpoint inhibition and single fraction stereotactic radiosurgery in brain metastases from non-small cell lung cancer: an international multicenter study of 395 patients", J Neurooncol **165**, 63–77 (2023).

[80]R. Upadhyay, A. S. Ayan, S. Jain, B. G. Klamer, H. K. Perlow, W. Zoller, D. M. Blakaj, S. Beyer, J. Grecula, A. Arnett, E. Thomas, A. Chakravarti, R. R. Raval, and J. D. Palmer, "Dose-volume tolerance of the brain and predictors of radiation necrosis after 3-fraction radiosurgery for brain metastases: a large single-institutional analysis", International Journal of Radiation Oncology*Biology*Physics **118**, 275–284 (2024).

[81]P. K. Sneed, J. Mendez, J. G. M. Vemer-van Den Hoek, Z. A. Seymour, L. Ma, A. M. Molinaro, S. E. Fogh, J. L. Nakamura, and M. W. McDermott, "Adverse radiation effect after stereotactic radiosurgery for brain metastases: incidence, time course, and risk factors", JNS **123**, 373–386 (2015).

[82]M. Doré, S. Martin, G. Delpon, K. Clément, L. Campion, and F. Thillays, "Stereotactic radiotherapy following surgery for brain metastasis: predictive factors for local control and radionecrosis", Cancer/Radiothérapie **21**, 4–9 (2017).

[83]H. K. Inoue, K.-i. Seto, A. Nozaki, K. Torikai, Y. Suzuki, J.-i. Saitoh, S.-e. Noda, and T. Nakano, "Three-fraction CyberKnife radiotherapy for brain metastases in critical areas: referring to the risk evaluating radiation necrosis and the surrounding brain volumes circumscribed with a single dose equivalence of 14 gy (v14)", Journal of Radiation Research **54**, 727–735 (2013).

[84]B. Bengt K. Lind Panayiotis Mavroidis, "Optimization of the dose level for a given treatment plan to maximize the complication-free tumor cure", Acta Oncologica **38**, 787–798 (1999).

[85]"Effect of radiotherapy after breast-conserving surgery on 10-year recurrence and 15-year breast cancer death: meta-analysis of individual patient data for 10 801 women in 17 randomised trials", The Lancet **378**, 1707–1716 (2011).

[86]J. M. Taylor, W. M. Mendenhall, and R. S. Lavey, "Dose, time, and fraction size issues for late effects in head and neck cancers", International Journal of Radiation Oncology*Biology*Physics **22**, 3–11 (1992).

[87]R. Chappelg, D. M. Nondahl, M. Rezvani, and J. F. Fowler, "Further analysis of radiobiological parameters from the first and second british institute of radiology randomized studies of larynx/pharynx radiotherapy", International Journal of Radiation Oncology*Biology*Physics **33**, 509–518 (1995).

[88]X. S. Qi, J. White, and X. A. Li, "Is / for breast cancer really low?", Radiotherapy and Oncology **100**, 282–288 (2011).

[89]A. Murray Brunt, J. S. Haviland, D. A. Wheatley, M. A. Sydenham, A. Alhasso, D. J. Bloomfield, C. Chan, M. Churn, S. Cleator, C. E. Coles, A. Goodman, A. Harnett, P. Hopwood, A. M. Kirby, C. C. Kirwan, C. Morris, Z. Nabi, E. Sawyer, N. Somaiah, L. Stones, I. Syndikus, J. M. Bliss, J. R. Yarnold, A. Alhasso, A. Armstrong, J. Bliss, D. Bloomfield, J. Bowen, M. Brunt, C. Chan, H. Chantler, M. Churn, S. Cleator, C. Coles, E. Donovan, A. Goodman, S. Griffin, J. Haviland, P. Hopwood, A. Kirby, J. Kirk, C. Kirwan, M. MacLennan, C. Morris, Z. Nabi, E. Sawyer, M. Sculphur, J. Sinclair, N. Somaiah, L. Stones, M. Sydenham, I. Syndikus, J. Tremlett, K. Venables, D. Wheatley, and J. Yarnold, "Hypofractionated breast radiotherapy for 1 week versus 3 weeks (FAST-forward): 5-year efficacy and late normal tissue effects results from a multicentre, non-inferiority, randomised, phase 3 trial", The Lancet **395**, 1613–1626 (2020).

[90]J. S. Haviland, J. R. Owen, J. A. Dewar, R. K. Agrawal, J. Barrett, P. J. Barrett-Lee, H. J. Dobbs, P. Hopwood, P. A. Lawton, B. J. Magee, J. Mills, S. Simmons, M. A. Sydenham, K. Venables, J. M. Bliss, and J. R. Yarnold, "The UK standardisation of breast radiotherapy (START) trials of radiotherapy hypofractionation for treatment of early breast cancer: 10-year follow-up results of two randomised controlled trials", The Lancet Oncology **14**, 1086–1094 (2013).

[91]F. Liu, J. D. Ververs, M. K. Farris, A. W. Blackstock, and M. T. Munley, "Optimal radiation therapy fractionation regimens for early-stage non-small cell lung cancer", International Journal of Radiation Oncology*Biology*Physics **118**, 829–838 (2024).

[92]B. Maciejewski, H. Withers, J. M. Taylor, and A. Hliniak, "Dose fractionation and regeneration in radiotherapy for cancer of the oral cavity and oropharynx: tumor dose-response and repopulation", International Journal of Radiation Oncology*Biology*Physics **16**, 831–843 (1989).

[93]P. Gut, S. Hayoz, K. Kothbauer, P. Thum, and R. Seiler, "Ablative radiotherapy to brain metastasis and dose intensified radiotherapy to resection cavity combined with low dose whole brain irradiation using volumetric modulated arc therapy", Personal communication (2016).

Declaration of Authorship

I hereby declare that, to the best of my knowledge and belief, this thesis titled *Application of a Closed-Form Population-Based Tumor Control Probability Model* is my own, independent work. I confirm that each significant contribution to and quotation in this thesis that originates from the work or works of others is indicated by proper use of citation and references; this also holds for tables and graphical works.

Zurich, 05.12.2024

Sara Erni

Unless explicitly specified otherwise, this work is licensed under the license Attribution-ShareAlike 4.0 International.